ACS Biomaterials SCIENCE & ENGINEERING

pubs.acs.org/journal/abseba

Article

A Three-Dimensional Printable Hydrogel Formulation for the Local Delivery of Therapeutic Nanoparticles to Cervical Cancer

Mariia Kiseleva, Mahmoud M. Omar, Élodie Boisselier, Svetlana V. Selivanova, and Marc-André Fortin*

Cite This: *ACS Biomater. Sci. Eng.* 2022, 8, 1200−1214

Read Online

ACCESS | Metrics & More | Article Recommendations | Supporting Information

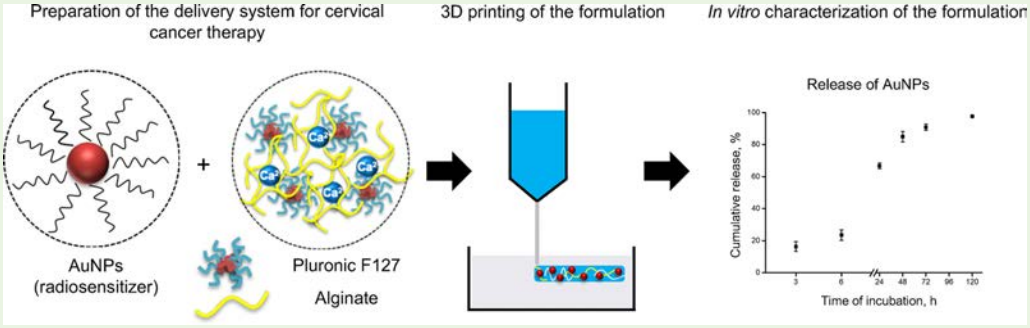

ABSTRACT: Cervical cancer is the fourth most common malignancy among women. Compared to other types of cancer, therapeutic agents can be administrated locally at the mucosal vaginal membrane. Thermosensitive gels have been developed over the years for contraception or for the treatment of bacterial, fungal, and sexually transmitted infections. These formulations often carry therapeutic nanoparticles and are now being considered in the arsenal of tools for oncology. They can also be three-dimensionally (3D) printed for a better geometrical adjustment to the anatomy of the patient, thus enhancing the local delivery treatment. In this study, a localized delivery system composed of a Pluronic F127-alginate hydrogel with efficient nanoparticle (NP) release properties was prepared for intravaginal application procedures. The kinetics of hydrogel degradation and its NP releasing properties were demonstrated with ultrasmall gold nanoparticles (~80% of encapsulated AuNPs released in 48 h). The mucoadhesive properties of the hydrogel formulation were assayed by the periodic acid/Schiff reagent staining, which revealed that 19% of mucins were adsorbed on the gel's surface. The hydrogel formulation was tested for cytocompatibility in three cell lines (HeLa, CRL 2616, and BT-474; no sign of cytotoxicity revealed). The release of AuNPs from the hydrogel and their accumulation in vaginal membranes were quantitatively measured *in vitro*/*ex vivo* with positron emission tomography, a highly sensitive modality allowing real-time imaging of nanoparticle diffusion (lag time to start of permeation of 3.3 h, 47% of AuNPs accumulated in the mucosa after 42 h). Finally, the potential of the AuNP-containing Pluronic F127-alginate hydrogel for 3D printing was demonstrated, and the geometrical precision of the 3D printed systems was measured by magnetic resonance imaging (<0.5 mm precision; deviation from the design values <2.5%). In summary, this study demonstrates the potential of Pluronic F127-alginate formulations for the topical administration of NP-releasing gels applied to vaginal wall therapy. This technology could open new possibilities for photothermal and radiosensitizing oncology applications.

KEYWORDS: *vaginal localized delivery, hydrogel, Pluronic F127, alginate, cervical cancer therapy, gold nanoparticles, 3D printing*

INTRODUCTION

Cervical cancer is the fourth most common malignancy among women with over 200,000 deaths worldwide annually and the leading cause of cancer mortality among women in developing countries.[1] In developed countries, vaccination has had a strong effect on the total number of cases. However, according to the World Health Organization, by 2045, the number of deaths from cervical cancer is nonetheless expected to increase nearly by 2.5.[2] In the mid-term, vaccination alone is not expected to represent the sole medical weapon in the arsenal against cervical cancer, and innovative therapies are welcomed in the field.

Compared with certain types of cancer localized in deeper organs, the cervix is easily accessible through the vagina. In fact, a variety of dosage forms have already been developed for purposes such as contraception and for the treatment of

Received: November 3, 2021
Accepted: February 8, 2022
Published: February 28, 2022

https://doi.org/10.1021/acsbiomaterials.1c01399
ACS Biomater. Sci. Eng. 2022, 8, 1200−1214

bacterial, fungal, or sexually transmitted infections.[3] Therefore, local cancer resection and localized delivery can be used in many cases to treat the malignancy at early stages when cancer is still confined to the cervix.[3,4] Therapeutic agents (chemotherapeutics, immunotherapeutics, or radiosensitizers) can be applied at the surface of the cervix either as a primary treatment or as a complementary preventive procedure.[5,6]

Many hydrogels very well tolerated by patients, have been developed for vaginal wall applications.[1] More specifically, thermosensitive in situ forming gel formulations are increasingly being considered for intravaginal drug delivery.[2,7] These polymeric solutions undergo a sol−gel transition upon warming above a specific temperature known as the low critical gelation temperature (LCGT). Thermosensitive polymers with a LCGT close to 37 °C are of particular interest as they can flow through a needle or an applicator to form a viscous gel upon contact with the vaginal wall. Among them, poloxamers such as Pluronics are the most widely used reverse thermal gelation polymers in drug delivery.[8,9] Pluronic F127 (PF127) is approved by the health authorities (*e.g.*, FDA, Health Canada, and European Medicines Agency) for dental, nasal, and topical routes of administration.[10] It is also listed in the U.S. and European pharmacopeia as a gelling agent for vaginal formulations (a maximum permissible concentration is 50% w/w).[11]

However, these formulations are associated with certain limitations. First, in situ gelation is not an instantaneous process; depending on a composition of the formulation and its physicochemical characteristics, a polymer system can require 1−2 min to complete a transition to solid or semisolid depot.[12] Consequently, a considerable amount of encapsulated therapeutics can leak out and be lost during gel formation.[4] Moreover, a high variability in the final shape, size, and structure of the formed object or layer is expected from one injection to another.[13] The speed of injection and type of needle or device used for the procedure all affect the final properties of the formed implant.[13]

Gel printing (*i.e.*, three-dimensional (3D) printing) provides an opportunity for developing more personalized hydrogels for topical applications, including for cervical cancer. It has been demonstrated that hydrogels can be printed in a variety of different shapes mimicking the contours of the cancerous area.[14] Through a 3D shaped system adapted to the anatomy of the patient and to the form of the vaginal wall lesions to be treated, therapeutic doses could be tailored with specific shapes and/or sizes according to the patient's needs.[15] Moreover, patients who have already been through surgery procedures leaving scars or resections on their gynecological tissues could specifically benefit from personalized 3D printed systems since they can be shaped to carefully delineate the application surface.[16] Until now, the scientific literature on the development of 3D printed hydrogels for the treatment of cervical cancer has been scarce.

In this study, a new thermosensitive hydrogel formulation containing a poloxamer (PF127), alginate, and therapeutic gold nanoparticles (AuNPs) was developed for 3D printing applications oriented toward cervical cancer therapy. PF127 is a synthetic thermosensitive polymer that can form a gel phase at a temperature close to 37 °C by physical cross-linking.[17] This phase transition behavior makes PF127 ideal for patterning structures in 3D printing with high resolution.[18] Alginate is a natural anionic polysaccharide that undergoes gelation through the chelation of Ca^{2+} ions by the carboxylic acid groups on adjacent strands of the β-D-mannuronate or α-L-guluronate epimers.[19] Ionic cross-linking provides excellent structural fidelity and improves the mechanical stiffness of the formed gel system. Moreover, high mucoadhesive properties of alginate could improve the residence time of the gel formulation in the cervix.[20] Here, AuNPs were used both for their therapeutic potential and as a model for other types of therapeutic NPs (*e.g.*, drug-releasing nanoparticles).[21] AuNPs can be used as a photothermal conversion material in photothermal therapy (PTT) as well as a radiosensitizer in radiotherapy.[22,23] Both therapeutic strategies, in addition to the surgical resection and chemotherapy, could be used to eliminate cancerous cells.[22,24]

Through a combination of different physicochemical characterization techniques (ultraviolet−visible spectroscopy (UV−vis), micro-X-ray fluorescence imaging, scanning electron microscopy (SEM), and Fourier-transform infrared spectroscopy (FTIR)), the hydrogel formulations were characterized in terms of their sol−gel behavior followed by *in vitro* degradation and AuNP release tests. Then, the mucoadhesive potential of the gels was investigated by a periodic acid/Schiff (PAS) colorimetric method followed by cytotoxicity tests (with human cervical cancer, human normal vaginal mucosa, and human breast cancer cell lines). The kinetics of AuNP accumulation in vaginal membranes (porcine) was measured *in vitro*/*ex vivo* by the diffusion cell coupled to a high-sensitivity detection system (PET). Finally, hydrogel scaffolds were 3D printed in two different shapes followed by magnetic resonance imaging (MRI) for visualization and measurement purposes (accuracy and reproducibility). These experiments demonstrated the potential of hydrogels based on Pluronic-alginate to be used for 3D printed NP-eluting oncology devices and systems.

MATERIALS AND METHODS

Reagents and Chemicals. *AuNP Synthesis.* Deferoxamine mesylate salt (DFO, $C_{25}H_{48}N_6O_8{\cdot}CH_4O_3S$, 659.79 g/mol, ≥92.5%), sodium borohydride ($NaBH_4$, 37.83 g/mol, 99.99% trace metal basis), and tetrachloroaurate ($HAuCl_4{\cdot}3H_2O$, 393.83 g/mol, ≥99.9% trace metal basis, 0.5 g/mL) were purchased from Millipore Sigma (Oakville, Canada). Thiol-polyethylene glycol-NHS (HS-PEG-NHS, 1000 Da, ≥95.0%) was obtained from Biochempeg Scientific Inc. (Watertown, USA).

Hydrogel Preparation, Degradation Tests, and 3D Printing. Pluronic F127 (PF127, 12,600 g/mol, suitable for cell culture), alginic acid sodium salt (120,000−190,000 g/mol; ratio of mannuronic acid to guluronic acid: 1.56), calcium chloride ($CaCl_2$, 110.98 g/mol, ≥93.0%), and hydrogen peroxide solution (H_2O_2, ≥30.0%, for trace analysis) were purchased from Millipore Sigma (Oakville, Canada). Throughout the experiments, all concentrations of polymer solutions are given in weight/volume percentages (% w/v) unless indicated otherwise. For *in vitro* hydrogel degradation and AuNP release tests, simulated vaginal fluid (SVF) was used as a dissolution medium and was prepared as previously described.[25] Briefly, sodium chloride (NaCl, 58.44 g/mol, ≥99.0%, 3.51 g), potassium hydroxide (KOH, 56.11 g/mol, ≥85.0%, 1.4 g), calcium hydroxide ($Ca(OH)_2$, 74.09 g/mol, ≥95.0%, 0.22 g), bovine serum albumin (lyophilized powder, ≥96.0%, 0.018 g), lactic acid ($C_3H_6O_3$, 90.08 g/mL, ≥85.0%, 2.00 g), acetic acid ($C_2H_4O_2$, 60.05 g/mol, ≥99.0%, 1.00 g), glycerol ($C_3H_8O_3$, 92.09 g/mol, ≥99.0%, 0.16 g), urea (negative urine control, 0.4 g), and glucose ($C_6H_{12}O_6$, 180.16 g/mol, ≥96.0%, 5.00 g), all purchased from Millipore Sigma (Oakville, Canada), were added to 900 mL of nanopure water and stirred until complete dissolution. The pH of the mixture was adjusted to 4.5 using 0.1 N HCl, and the final volume was adjusted to 1 L using nanopure water (water purifier: Purelab Flex, ELGA LabWater).

https://doi.org/10.1021/acsbiomaterials.1c01399
ACS Biomater. Sci. Eng. 2022, 8, 1200−1214

Hydrogel Cytotoxicity and Biocompatibility Tests. Normal human vaginal mucosa (CRL 2616) and human breast cancer (BT-474) cell lines were purchased from American Type Culture Collection (ATCC, USA). Human cervical cancer (HeLa) cells were kindly provided by Dr. René C. Gaudreault and Dr. Sébastien Fortin (from the Centre de Recherche du CHU de Québec − Université Laval). Fetal bovine serum, 0.5% Trypsin−EDTA (10×), penicillin (10,000 units/mL)−streptomycin (10,000 μg/mL), phosphate buffered saline 1×, a Roswell Park Memorial Institute medium (RPMI 1640) supplemented with L-glutamine, keratinocyte-serum free media supplemented with human recombinant epidermal growth factor, and bovine pituitary extract (BPE) were purchased from Gibco, Thermo Fisher Scientific (Canada). Dulbecco's modified Eagle's medium/Ham's nutrient mixture F12, Dulbecco's modified Eagle's medium (DMEM) with a high glucose content, calcium chloride solution (0.5 M, suitable for cell culture), and insulin solution from the bovine pancreas (1 mg/mL, in 25 mM HEPES, pH 8.2, suitable for cell culture) were obtained from Millipore Sigma (Oakville, Canada).

Mucin Adsorption Tests. All reagents for these tests (pararosaniline hydrochloride, sodium metabisulfite, and concentrated periodic acid) were kindly provided by Dr. Élodie Boisselier's research laboratory. Pararosaniline hydrochloride ($C_{19}H_{18}ClN_3$, 323.82 g/mol, >90.0%) and sodium metabisulfite ($Na_2S_2O_5$, 190.11 g/mol, ≥97.0%) were obtained from VWR International. Periodic acid (H_5IO_6, 227.94 g/mol, 99%) was purchased from Sigma-Aldrich (St. Louis, MO). A stock solution of mucin was prepared by dissolving mucin powder from a porcine stomach (Type III, bound sialic acid 0.5−1.5%, partially purified powder; Millipore Sigma, Oakville, Canada) in nanopure water to a final concentration of 1 mg/mL, sonicated for 30 min (Fisher Scientific FS30 Ultrasonic Cleaner), and filtered through a 0.45 μm syringe filter (polypropylene EZFlow syringe filter, 13 mm diameter, 0.45 μm pore size, Foxx Life Sciences).

Diffusion Cell Experiments. [^{89}Zr]Zr-oxalate ($t_{1/2}$ = 78.41 h, C_4O_8Zr, 265 g/mol, 1350 MBq/mL) was purchased from the University of Alabama (Birmingham, USA). Radioactivity measurements were performed using a calibrated dose calibrator (Atomlab 100, Biodex Medical Systems, Shirley, USA). Oxalic acid ($C_2H_2O_4$, 90.03 g/mol, 99.999% trace metals basis), sodium carbonate (Na_2CO_3, 105.99 g/mol, anhydrous, 99.999% trace metals basis), and ethylenediaminetetraacetic acid (EDTA, disodium salt, dihydrate, $C_{10}H_{16}N_2O_8$, 372.24 g/mol) were purchased from Millipore Sigma. 4-(2-Hydroxyethyl)-1-piperazineethanesulfonic acid (HEPES, $C_8H_{18}N_2O_4S$, 238.3 g/mol) was obtained from Fisher BioReagents. Phosphate buffered saline (PBS) (pH 7.4) was purchased from Gibco by Life Technologies (Grand Island, USA). Silica gel thin-layer chromatography plates (TLC silica gel 60 F254) were purchased from Millipore (catalog number 105715, Canada). All solutions were prepared with ultrapure water (OmniTrace Ultra, for trace metal analysis, Millipore) to minimize potential contamination with metal ions. Where needed, pH of the solutions was adjusted with NaOH (5 mol/L) or HCL (5 mol/L) and verified using pH paper (catalog number BDH35311.604, VWR Chemicals BDH, Canada). Porcine vaginal membranes were obtained from a local slaughterhouse and were stored-frozen.

Methods. *AuNP Synthesis.* The synthesis and characterization procedures of gold nanoparticles (AuNPs-PEG-DFO) are described in the Supporting Information, Section S1.

Hydrogel Preparation, Physicochemical Characterization, and Formulation Tests. Polymer solutions were prepared by dissolving PF127 powder at predefined concentrations (% w/v) in deionized water at 4 °C to avoid gelation during solution preparation.[26] When needed, alginate at a concentration of 1% w/v was added to PF127 homogeneous solution. Final concentrations of the PF127 and alginate components in the polymer solution were 20 and 1% w/v, respectively. The polymer solutions were kept at 4 °C overnight before beginning the experiments. When needed, AuNPs-PEG-DFO was mixed at a concentration of 15 mmol/L (based on the Au content) with a PF127-alginate polymer solution for 1 h at 4 °C.

Tube Inversion Test. The sol−gel−sol phase transition behavior of aqueous PF127 solutions was investigated using the tube inversion method. Solutions with a PF127 concentration ranging between 15 and 40% w/v were tested. Each sample was subjected to a controlled temperature increase from 4 to 99 °C in an Eppendorf Thermomixer Compact (Sigma-Aldrich). Each step consisted of a 1 °C temperature increase followed by isothermal maintenance for 5 min and tube inversion that allowed visual inspection of the occurrence of the phase transition. The sol and the gel were identified in a 30 s inspection as "flow liquid sol" and "no flow solid gel", respectively.

Gelation Time Test. The gelation time test of aqueous PF127 solutions at a physiological temperature (37 °C) is described in the Supporting Information, Section S2.

In Vitro Degradation Study. The "membrane-less" model was used to evaluate the *in vitro* erosion of the PF127-alginate hydrogel.[7,27] Flat-bottomed vials with an effective dissolution area of 6 cm^2 containing 1.5 g of polymer solution were incubated in a thermostatic shaker (Lab-Line Environ Orbital Model Shaker) set at 37 °C for 10 min to allow the polymer solution to form a gel phase. Then, $CaCl_2$ solution (0.1 mol/L, 2 mL) was added to complete the gelation process by ionic cross-linking of alginate chains. After 10 min, the $CaCl_2$ solution was removed, and the hydrogel was rinsed with water pre-heated at 37 °C to remove $CaCl_2$ in excess. The dissolution medium (SVF, pH 4.5, 10 mL) pre-heated at 37 °C was layered over the upper surface of the hydrogel. Then, a thermostatic shaker was set at 100 rpm. At pre-determined time points (3, 6, 24, 48, 72, and 120 h), all the dissolution medium was taken out, and the hydrogels were rinsed with pre-heated water to remove the salts from the SVF medium from the surface. The outer surface of the vial was wiped dry, and the samples were lyophilized for 24 h (freeze dry system Lyph-Lock 6, Labconco) and weighted (dry mass measurements). The residual mass was calculated using the following equation:

$$\frac{W_t}{W_0}\cdot 100\% \tag{1}$$

where W_0 is a dry mass at time $t = 0$ (intact samples) and W_t is the dry mass at time t. Each time point was repeated in triplicate.

Fourier-Transform Infrared Spectroscopy (FTIR). The freeze-dried gel samples at different time points of degradation were fixed on a Si crystal and measured with an attenuated total reflection FTIR system (Agilent Cary 660 FTIR, Agilent Technologies, USA) equipped with a deuterated L-alanine-doped triglycine sulfate (DLa-TGS) detector and a Ge-coated KBr beam splitter. Spectra were recorded in an absorbance mode with 64 scans and a spectral resolution of 2 cm^{-1}.

Scanning Electron Microscopy (SEM). Morphological examination of the gels at different time points of degradation was performed using SEM apparatus Quanta 250 (FEI Company Inc., Thermo Fisher Scientific). For the analysis, gels were plunged into liquid nitrogen for 10 min and lyophilized for 24 h. Samples were prepared by fixing the lyophilized hydrogel scaffolds to a holder using a conducting carbon strip, without further coating. The samples were analyzed at a 3 kV electron beam and a spot size of 3 μm at 200−1000× magnification. Pore size analysis was then performed on at least 100 pores with an ImageJ software.

Micro-X-ray Fluorescence Imaging. The distribution of Au and Ca atoms within the PF127-alginate hydrogel was visualized by micro-X-ray fluorescence (micro-XRF) imaging (M4 Tornado spectrometer (Bruker), equipped with a Rh anode X-ray tube (50 kV, 600 μA)). The analysis was performed on the lyophilized samples over an area of 15 × 15 mm, with an acquisition time of 5 ms per pixel and a spot size of 20 μm. The distribution of Au and Ca atoms was displayed by plotting images of the element's peak intensity at each pixel position.

In Vitro Release of AuNPs from Hydrogels. The "membrane-less" model described above was used. Flat-bottomed vials with an effective dissolution area of 6 cm^2 and containing AuNP-polymer solution were incubated in a thermostatic shaker set at 37 °C for 10 min to allow the polymer solution to form a hydrogel. Then, $CaCl_2$ solution (0.1 mol/L, 2 mL) was added to complete the gelation process. After 10 min, the $CaCl_2$ solution was removed, and the formed hydrogel was rinsed

https://doi.org/10.1021/acsbiomaterials.1c01399
ACS Biomater. Sci. Eng. 2022, 8, 1200−1214

with water pre-heated at 37 °C. The dissolution medium (SVF, pH 4.5, 10 mL) pre-heated at 37 °C was layered over the upper surface of the hydrogel. The vials were placed in a thermostatic shaker set at 37 °C and 100 rpm. At pre-determined time points (3, 6, 24, 48, 72, and 120 h), an aliquot (0.5 mL) of the dissolution medium was taken out and the vial was replenished with fresh buffer. UV−visible light absorption spectra were obtained using a Shimadzu UV-1601 spectrophotometer over the spectral range of 400−600 nm (using a quartz cell). To evaluate the concentration of AuNPs-PEG-DFO in the release medium, a calibration curve was plotted between known concentrations of NPs and the intensity of the plasmon peak (510 nm) from UV−vis measurements (see the Supporting Information, Section S5, Figure S5).

The release profile of AuNPs-PEG-DFO from the gel was analyzed with the power-law model

$$\frac{M_t}{M_\infty} = kt^n \tag{2}$$

where M_t and M_∞ are the absolute cumulative amount of AuNPs-PEG-DFO released at time t and infinite time, respectively, and k is a constant incorporating structural and geometric characteristics of the device.[27] By fitting the data of M_t, M_∞, and t into this equation, the release exponent n was calculated to reveal the mechanism of NP release.

Swelling Ratio. The freeze-dried gel samples at $t = 0$ from the *in vitro* degradation study described above were further used to determine the swelling ratio of the gels in SVF (pH 4.5). The samples were incubated in SVF (10 mL) in the flat-bottomed vials at 37 °C and 50 rpm (to avoid possible disintegration of the samples) in a thermostatic shaker. At pre-determined time points (30 min, 1, 2, 3, and 4 h), the incubation medium was discarded, the outer surface of the vial was wiped dry with filter paper, and the mass of the swelled gels was noted down. The swelling ratio of the gels in SVF was calculated as

$$\frac{W_{\text{swelled}} - W_{\text{dry}}}{W_{\text{dry}}} \cdot 100\% \tag{3}$$

where W_{swelled} is a mass of a swelled gel at time t and W_{dry} is a dry mass at time $t = 0$. To compare the swelling behavior of the PF127-alginate samples with literature data found for the polymers that are widely used for the preparation of vaginal applications, the mass swelling factor (MSF) was also calculated as

$$\text{MSF} = \frac{W_{\text{swelled}}}{W_{\text{dry}}} \tag{4}$$

Hydrogel Biocompatibility and Bio-Functionality Tests: Cell Viability, Contact Assays, Mucin Adsorption, and Membrane Diffusion Tests. *Cell Culture.* HeLa cells were maintained in DMEM supplemented with fetal bovine serum (10%) and antibiotic solution (penicillin−streptomycin, 1%). CRL 2616 cells were maintained in keratinocyte-serum free media with human recombinant EGF (0.1 ng/mL), bovine pituitary extract (0.05 mg/mL), antibiotic solution (penicillin−streptomycin, 1%), and additional calcium chloride (44.1 mg/L, a final concentration of 0.4 mM). BT-474 cells were maintained in an RPMI medium supplemented with fetal bovine serum (10%), antibiotic solution (penicillin−streptomycin, 1%), and insulin (0.1%). All cell lines were maintained at 37 °C in a saturated humid atmospheric chamber containing 95% air and 5% CO_2. Once confluent, the cells were detached from the flask with Trypsin−EDTA (0.05%), centrifuged, counted, and then resuspended in the growth medium for further experiments. Each condition of the cell culture experiments was repeated six times.

Direct Cell Contact Assays. The effect of the PF127-alginate formulation and its individual components on cell viability was assessed using the following protocol.[28,29] PF127 20% w/v-alginate 1% w/v, PF127 20% w/v, and alginate 1% w/v polymer solutions were sterilized by autoclaving at 120 °C for 45 min. The tested cells were trypsinized, centrifuged, and resuspended at a density of 1×10^6 cells/mL in the culture medium. The cell suspension was added into each well (1×10^5 cells/well for CRL-2616 cells, 2×10^5 cells/well for HeLa cells, and 5×10^5 cells/well for BT-474 cells) and incubated in 5% CO_2 at 37 °C for 24 h. Then, polymer solution samples (500 μL) were layered over the cells and incubated at 37 °C for 2 min. At this point, a thin gel film was formed in the well plates containing PF127 20% w/v-alginate 1% w/v and PF127 20% w/v samples due to the sol−gel transition of the PF127 component. Then, $CaCl_2$ (0.1 mol/L, 100 μL) was added to the well plates containing PF127 20% w/v-alginate 1% w/v and alginate 1% w/v to induce the ionic cross-linking of alginate, and the well plates were gently shaken for 5 min. The excess of $CaCl_2$ was discarded, and the formed gels were washed twice with PBS. The cell culture media (1 mL) were then added on top of the gels. Incubation was carried out in 5% CO_2 at 37 °C for 24 and 48 h. Control well plates containing the untreated cells in complete growth media and in media with 2% DMSO were used as a negative and a positive control, respectively (for BT-474 cells, only negative control was used). Cell viability was assessed by the trypan blue dye exclusion method.[30] For this, the cell culture medium was removed from the samples followed by washing the samples with PBS and cell trypsinization. The cells were then resuspended in culture media, and an aliquot (10 μL) of the cell suspension was taken and mixed with a trypan blue dye (10 μL). Cell viability was measured with a Cellometer Auto T4 cell counter (Nexcelom). The statistical differences between the control and experimental groups were analyzed according to the paired Student's t test. Statistical significances were presented when the p-values were less than 0.05 (*) and less than 0.005 (**). The data is given as mean ± standard deviation, $n = 6$.

Mucin Adsorption Tests by the Mucin Glycoprotein Assay (PAS Staining). A periodic acid/Schiff colorimetric method was used to assess the amount of mucin adsorbed on the gels. Two reagents were prepared. The Schiff reagent contained basic fuchsin (pararosaniline hydrochloride, aqueous solution, 1%, 100 mL) and hydrochloric acid (1 mol/L, 20 mL). Sodium metabisulfite (0.1 g) was added to every 6 mL of the Schiff reagent before use, and the resultant solution was incubated at 37 °C until it became colorless or pale yellow (2 h). The periodic acid reagent was freshly prepared by adding periodic acid (50%, 10 μL) solution to acetic acid solution (7% v/v, 7 mL). Mucin from the porcine stomach was dissolved at pre-defined concentrations in deionized water (0, 50, 75, 100, 125, and 150 μg/mL), and a standard calibration curve was obtained (see the Supporting Information, Section S7, Figure S8). A periodic acid reagent (180 μL) was added to the sample (600 μL). After 2 h of incubation at 37 °C, the Schiff reagent (60 μL) was added at room temperature. Thirty (30) minutes later, the absorbance of the solution was recorded at 575 nm using a UV−visible spectrometer. All the samples were analyzed with the same procedure. Flat-bottomed vials containing 1.5 g of the polymer solution were incubated in a thermostatic shaker set at 37 °C for 10 min to allow the polymer solution to form a gel phase. Then, $CaCl_2$ solution (0.1 mol/L, 2 mL) was added to complete the gelation process by ionic cross-linking of alginate chains. After 10 min, the $CaCl_2$ solution was removed. Mucin solution (100 μg/mL, 5 mL) pre-equilibrated at 37 °C was layered over the upper surface of the hydrogel. Incubation was carried out at 37 °C in a thermostatic shaker for 1 h at 50 rpm. After the incubation, the mucin solution was taken out and the mucin content was calculated from the standard calibration curve. Control samples containing only gels were also prepared. The experiment was performed in triplicate. The data is given as mean ± standard deviation, $n = 3$.

Membrane Diffusion and Accumulation Tests by PET Imaging. Aliquots of AuNPs were radiolabeled, as described in the Supporting Information, Section S1. Radiolabeled AuNPs ([^{89}Zr]Zr-AuNPs) were mixed by vortexing with the PF127-alginate polymer solution (20:1% w/v, respectively). The final concentration of [^{89}Zr]Zr-AuNPs in the gel was 0.1 mM (based on the Au content), and the radioactivity concentration was 2.6 MBq/mL. The Au concentration in the samples was measured by microwave plasma atomic emission spectrometry (MP-AES, Analyst 800, PerkinElmer). For this, each sample (25 μL) was digested with aqua regia (2 mL) for 2 h at 80 °C.

https://doi.org/10.1021/acsbiomaterials.1c01399
ACS Biomater. Sci. Eng. 2022, 8, 1200−1214

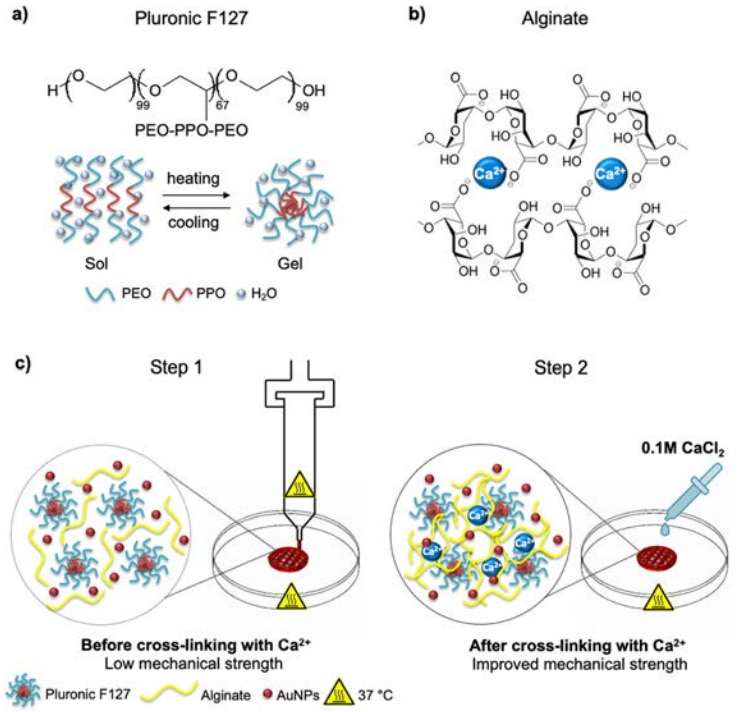

Figure 1. Schematic representations of the hydrogel formulation developed for nanoparticle-releasing 3D printed systems: (a) Pluronic F127; (b) alginate and its polymerization mechanism with Ca^{2+}. (c) Two-step 3D printing procedure for the lens-shaped scaffolds (see MRI results).

Then, H_2O_2 (1 mL) at 80 °C was added and left for digestion for 2 h. The experiment was performed in triplicate.

Hydrogel cylinders were 3D printed (see the procedure in the next section; diameter: 19 mm; height: 8 mm; 2.27 mL) to fit into the donor compartment (DC) of a diffusion cell operated in the PET scanner.[31] For operation in PET, the diffusion cell was specifically developed with materials transparent to γ-radiation (see the Supporting Information, Section S8, Figure S9).[31] A porcine vaginal mucous membrane (thickness: ~2 mm) was dissected, wetted with PBS (100 μL), and then clamped into the diffusion cell (the cross-sectional area was 314.16 mm^2), thus forming a barrier between the DC and the acceptor compartment (AC; filled with PBS, 6 mL). The radioactive 3D printed gel was placed carefully on the membrane, which was fixed between the donor and acceptor compartments. The cell was locked on the bed of the PET scanner (LabPETII scanner, IR&T, Sherbrooke, Canada) and kept at the center of the field of view (FOV) for the duration of the experiment. The diffusion cell was run in static mode and imaged continuously for 42 h. After the diffusion procedure, the remains of the hydrogel cylinder were removed from the DC, and the PBS collecting media in the AC was eliminated. The membrane was kept in place, gently washed several times with PBS, and reintroduced into the PET scanner. At the end of each acquisition, the data was reconstructed (20 iterations) with a voxel size of 0.3 × 0.3 × 0.3 mm and corrected for radioactivity decay and random events (no dead time, attenuation, or scatter correction applied). Image analysis and diffusion data extraction were performed according to a previously published procedure, which is also detailed in the Supporting Information, Section S8.[31]

Printability Assessment of AuNP-Containing Hydrogels. Numeric models of the scaffolds were designed using the FreeCAD software (0.19.2, OpenCasCade project, Germany). Hydrogel structures, including those used for the PET studies, were 3D printed using a Cellink Bio X extrusion-based system by a two-step procedure schematically demonstrated in Figure 1c.[18] The polymer solution was added at room temperature to the 3 mL printhead, equipped with a plastic nozzle with an inner diameter of 0.2 mm. The printhead was then heated up to 37 °C, which resulted in the rapid gelation of the PF127 component and the formation of the soft gel. Lens-shaped scaffolds (Ø 10 mm, h = 2 mm), hollow tube-shaped structures (Ø 3 mm, h = 3 mm), and the cylinders described for the PET procedures (above) were printed at an extrusion rate of 10 $mm{\cdot}s^{-1}$ with an applied pressure of 29 kPa on a Petri dish, which was fixed on a printer bed pre-heated at 37 °C. After printing, the soft gel structures were stabilized via ionic cross-linking of alginate chains (10 min immersion in 0.1 mol/L aqueous solution of $CaCl_2$ followed by rinsing in deionized water).

Visualization with Magnetic Resonance Imaging (MRI). The 3D printed hydrogels were visualized by MRI (1 T M2M, Aspect Imaging, Netanya, Israel). Lens-shaped scaffolds were inserted in a 3.5 cm diameter RF coil using a home-made 3D printed support and scanned using a T_1-weighted 2D spin echo sequence: FOV of 40 mm; 28 slices; 0.9 mm slice thickness; 0.1 mm slice gap; dwell time of 50 μs; matrix: 304 × 304; fα 90°; echo asymmetry of 50%; echo time/repetition time (TE/TR): 90/3167.2 ms; duration of 38 min. Hollow tube-shaped gels were inserted in a mouse head coil using a home-made 3D printed support and scanned using a T_1-weighted 2D spin echo sequence: FOV of 30 mm; 30 slices; 0.6 mm slice thickness; 0.1 mm slice gap; dwell time of 50 μs; matrix: 304 × 304; fα 90°; echo asymmetry of 50%; echo time/repetition time (TE/TR): 85/3250.9 ms; duration of 49 min 25 s. The images were then analyzed with ImageJ software.

The accuracy of 3D printing can be defined as a degree of agreement between the dimensions of the printed scaffold and the dimensions intended for the designed numeric model, which is an STL file.[32] Thus, this parameter was calculated by comparing the morphological features (diameter and height) of the printed gels measured by MRI and the designed models. The reproducibility of the gel geometry was evaluated by calculating the variability in size between the printed scaffolds (standard deviation; n = 3).

RESULTS

Hydrogel Preparation, Physicochemical Characterization, and Formulation Tests. Schematic representations

https://doi.org/10.1021/acsbiomaterials.1c01399
ACS Biomater. Sci. Eng. 2022, 8, 1200−1214

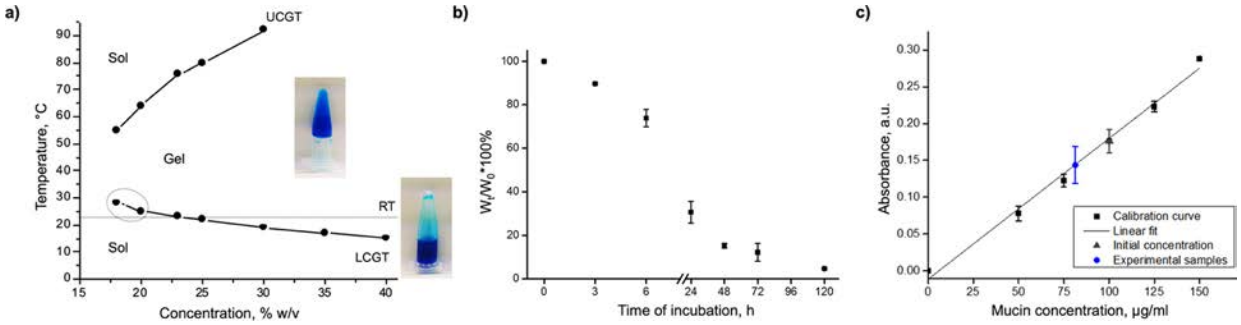

Figure 2. (a) Sol−gel behavior of Pluronic F127 aqueous solutions at different concentrations represented as a phase diagram; room temperature is indicated with the dashed line; LCGT, low critical gelation temperature; UCGT, upper critical gelation temperature. (b) *In vitro* degradation of the PF127 20% w/v-alginate 1% w/v hydrogel in SVF pH 4.5. Data are reported as mean ± standard deviation, $n = 3$. (c) Quantitative analysis of mucins adsorbed on the gel. The calibration curve of mucins is represented by black squares. The blue circle represents the percentage of free mucins after the incubation with the gel (an initial mucin concentration of 100 μg/mL, gray triangle). Data are reported as mean ± standard deviation, $n = 3$.

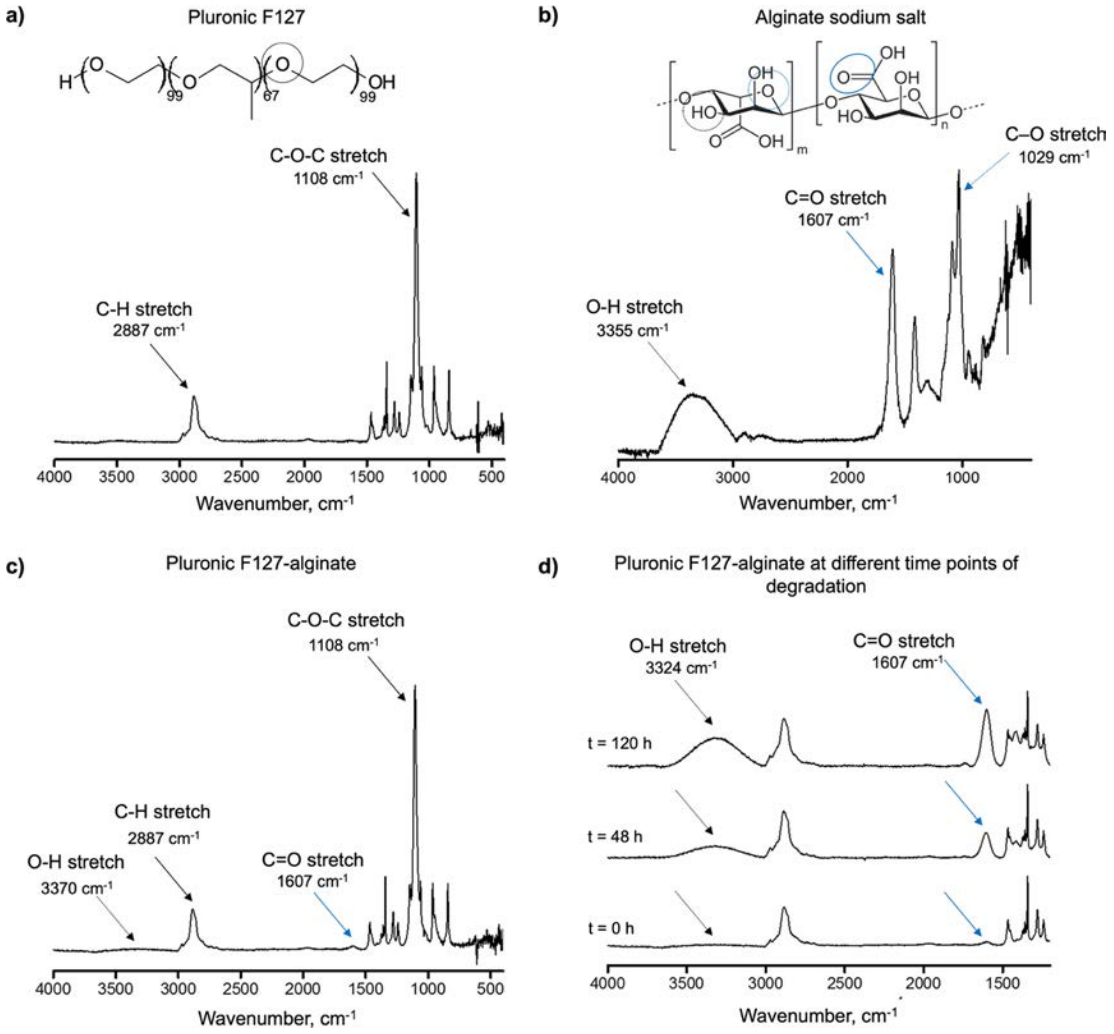

Figure 3. FTIR spectra of (a) Pluronic F127, powder; (b) alginate sodium salt, powder; (c) Pluronic F127 20% w/v-alginate 1% w/v mixture; (d) zoom-in of the FTIR spectra of the PF127 20% w/v-alginate 1% w/v gel at different time points of the degradation experiment.

of the hydrogel formulations composed of Pluronic (PF127), alginate, and AuNPs are shown in Figure 1. The process of hydrogel 3D printing and the gelation of the alginate component with calcium ions are also represented.

https://doi.org/10.1021/acsbiomaterials.1c01399
ACS Biomater. Sci. Eng. 2022, 8, 1200−1214

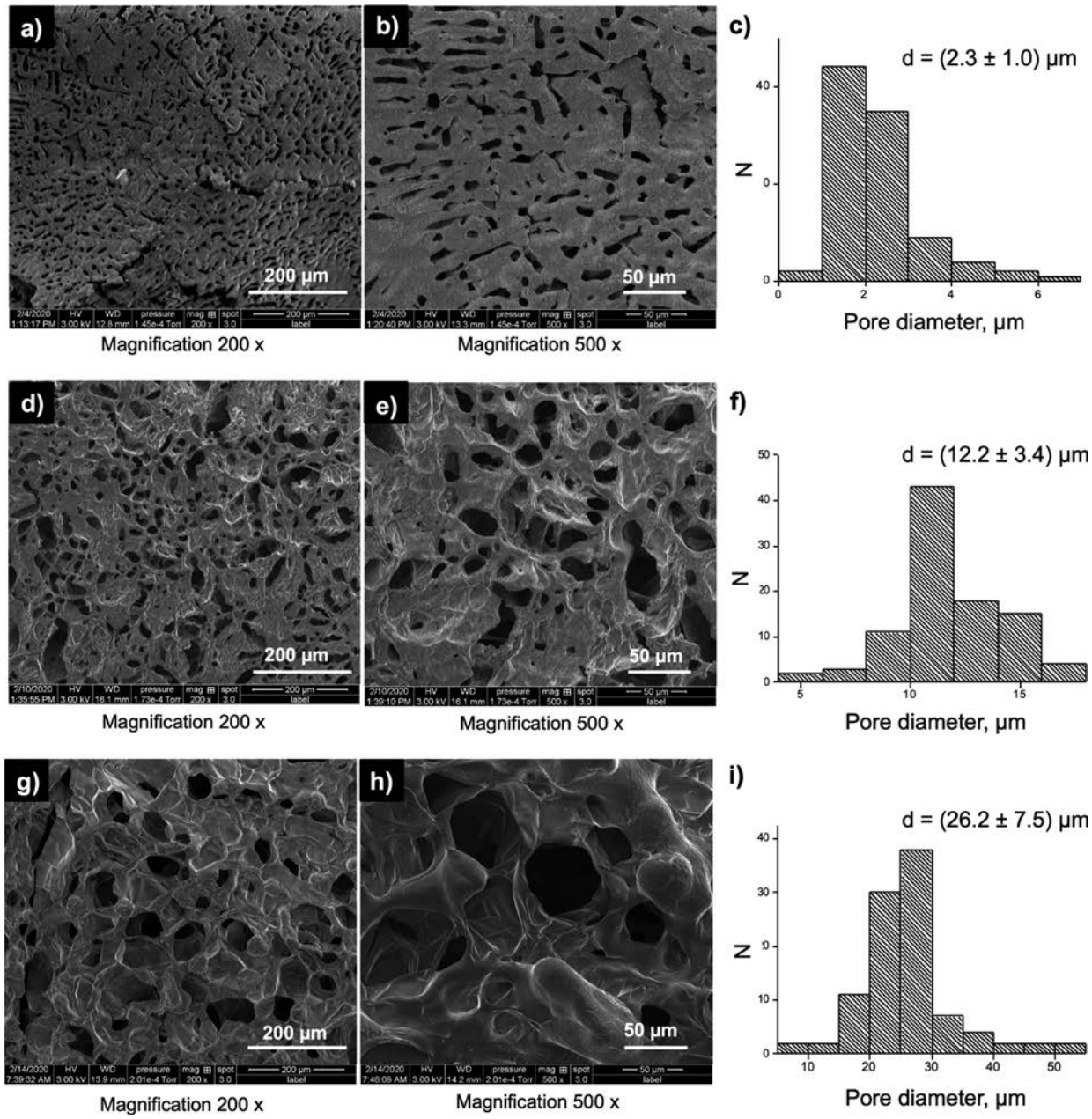

Figure 4. SEM images (3 keV) of the PF127-alginate sample and the distribution of the pore size (a–c) right after the preparation, (d–f) at 48 h post-degradation, and (g–i) at 120 h post-degradation.

Tube Inversion Test. PF127, the main component of the hydrogel, is a reverse thermosensitive polymer that undergoes a phase transition from liquid to a soft physical gel upon increasing the temperature.[33] The sol-to-gel transition temperature is the most fundamental parameter of the reversible polymers.[34] The low and upper critical gelation temperatures (LCGT and UCGT) of aqueous PF127 solutions were determined by a tube inversion test.[35,36] The phase diagram of PF127 at different concentrations ranging from 15 to 40% w/v is shown in Figure 2a.

The LCGT depends on the concentration of the PF127: the higher the concentration, the lower the gelation temperature. The phase diagram shows that the LCGT of the polymer solutions at 18 and 20% w/v (circled with a dashed line in Figure 2a) was higher than the room temperature (liquid at 22–23 °C and gel at higher temperatures). No gelation was observed under 15% w/v in the tested temperature range. At higher concentrations, the gel was formed at room temperature or below. Overall, these results demonstrate the possibility to perform all manipulations at room temperature without the risk of gelation (*e.g.*, encapsulation of NPs or drug molecules, addition of other polymers, and administration procedures involving needles), which is highly preferential for the medical applications of such hydrogel technologies.[36] PF127 at 20% w/

https://doi.org/10.1021/acsbiomaterials.1c01399
ACS Biomater. Sci. Eng. 2022, 8, 1200–1214

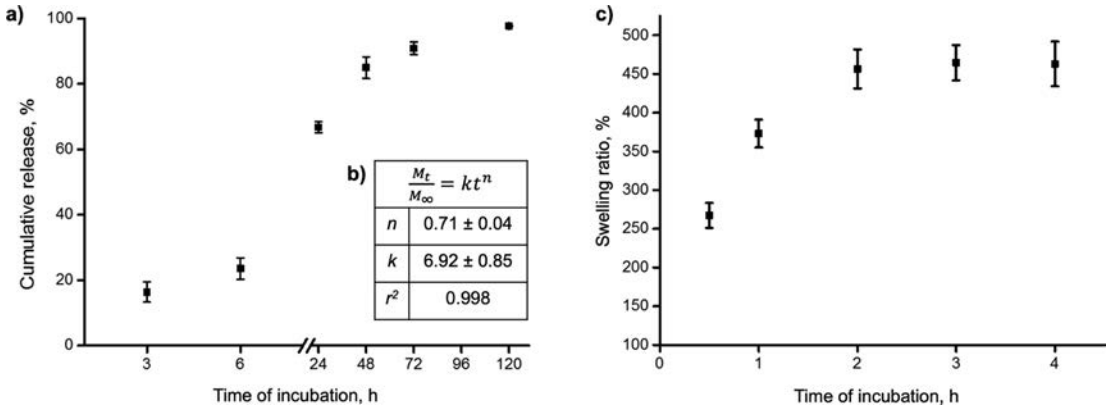

Figure 5. (a) Release of AuNPs from the PF127-alginate hydrogel *in vitro*. (b) The parameters *n*, *k*, and r^2 were found by fitting the release curves (power-law model). (c) Swelling ratio of the PF127-alginate hydrogel in SVF pH 4.5. Data are reported as mean ± standard deviation, $n = 3$.

v was chosen as the most optimal concentration for efficient gelation at 37 °C.

In Vitro Degradation Study and In Vitro Release of AuNPs from Hydrogels. *In vitro* degradation of the gels and *in vitro* release of AuNPs revealed the degradation and NP release kinetics in the perspective of *in vivo* applications. The ultrasmall AuNPs developed as the therapeutic component of the hydrogel formulation were of a spherical shape and narrow size distribution (TEM: 5.6 ± 2.5 nm; DLS: 18.5 ± 0.6 nm peak, intensity weighted, PDI index < 0.2, no evidence of large clusters, see the Supporting Information, Section S1, Figure S2). Successful grafting of PEG (for steric repulsion) and DFO (for ^{89}Zr chelation) on these particles was confirmed by FTIR (see the Supporting Information, Section S1, Figure S2d).

In vitro dissolution study of the PF127 20% w/v-alginate 1% w/v hydrogel was performed in SVF pH 4.5 to mimic the pH of the vaginal environment (3.8−4.5). The "membrane-less" method allows the release medium to be in direct contact with the gel surface, similar to *in vivo* conditions, where the gel would be exposed to the extracellular fluids.[37] The results of this experiment are presented in Figure 2b. As the graph reveals, the hydrogel mass gradually decreased during the experiment, with a higher degradation rate in the first (~2.5% per hour) and the second (~1% per hour) days and then at a slower rate (<1% per hour) until the end of incubation. The half-life of degradation was about 18 h, and the gels underwent complete dissolution in the incubation medium after 120 h. Similar results were found in the *in vitro* dissolution study using PBS as a dissolution medium (not reported in this article). The FTIR spectrum of a non-degraded PF127 20% w/v-alginate 1% w/v scaffold was dominated by the intense bands at 1108 cm^{-1} (ν_s(C−O−C) and ν_{as}(C−O−C)) and at 2887 cm^{-1} (ν(C−H, aliphatic)), typical of PF127 (identified with black arrows in Figure 3a,c). The presence of alginate in the system can be observed by the characteristic weak bands at 3370 cm^{-1} (ν(O−H)) and 1607 cm^{-1} (ν(C═O)) (identified with black dashed and blue arrows, see Figure 3b). Changes in the absorbance bands associated with the mannuronate and guluronate monomers of alginate (carboxylate stretch at 1607 cm^{-1} and hydroxyl group stretch at 3370 cm^{-1}) were monitored during the dissolution experiment. As can be seen from the spectra in Figure 3d, at 48 and 120 h post-incubation, the intensity of characteristic alginate peaks was greatly increased. This suggests that the *in vitro* degradation of the PF127-alginate scaffolds is governed by the rapid diffusion of the PF127 component out of the polymer network. PF127 is known for its fast dissolution rate in aqueous media that also can be explained by the loss of gel-like properties upon the influx of water that dilutes the polymer below its critical gelation concentration.[38]

The degradation of hydrogels at time points (t = 0, 48, and 120 h) during the dissolution process in SVF was also studied by SEM.

Directly after forming, the PF127-alginate gel had a uniform pore architecture (mean pore diameter: 2.3 ± 1.0 μm; Figure 4a,b). No evidence of phase separation was found in the SEM images, indicating a homogeneous blend of the PF127 and alginate components. However, upon elution of the PF127 component from the gel, the diameter of pores increased considerably, from 12.2 ± 3.4 μm at 48 h to 26.2 ± 7.05 μm at 120 h. Moreover, at 48 and 120 h, the gels exhibited a structure with aligned channels in the cross-sectional view (see the Supporting Information, Section S3, Figure S3). This can be explained by the progressive elution of the PF127 component that stabilized the formation of the microscopic pores.[18] Overall, the presence of micropores could facilitate the release of the encapsulated AuNPs from the gel network, and the hydrogel degradation kinetics matches the required time elution profile for the release of AuNPs for potential photothermal and radiotherapy treatments in cervix oncology.[39] Finally, micro-XRF spectroscopy mapping confirmed the homogeneous distribution of AuNPs and Ca (alginate cross-linker) in the as-prepared hydrogels. The spectrum of the as-prepared PF127-alginate gel with AuNPs (Supporting Information, Section S4, Figure S4a) revealed three peaks characteristic for Au (L_α 9.713, L_β 11.442, and M_α 2.123 keV) and two peaks characteristic for Ca (K_α 3.692 and K_β 4.013 keV). As can be seen from the Au mapping, Au atoms were uniformly present in the hydrogel sample, confirming the possibility to homogeneously distribute hydrophilic therapeutic NPs into this hydrogel formulation, which is a requirement for nanocomposite hydrogels.[40]

In vitro release of gold nanoparticles from the PF127-alginate hydrogel was investigated in the same experimental conditions as for the *in vitro* gel degradation tests (SVF, pH 4.5). Samples incubated for 120 h demonstrated that AuNPs were completely released into the dissolution medium (Supporting Information, Section S4, Figure S4b). On the

https://doi.org/10.1021/acsbiomaterials.1c01399
ACS Biomater. Sci. Eng. 2022, 8, 1200−1214

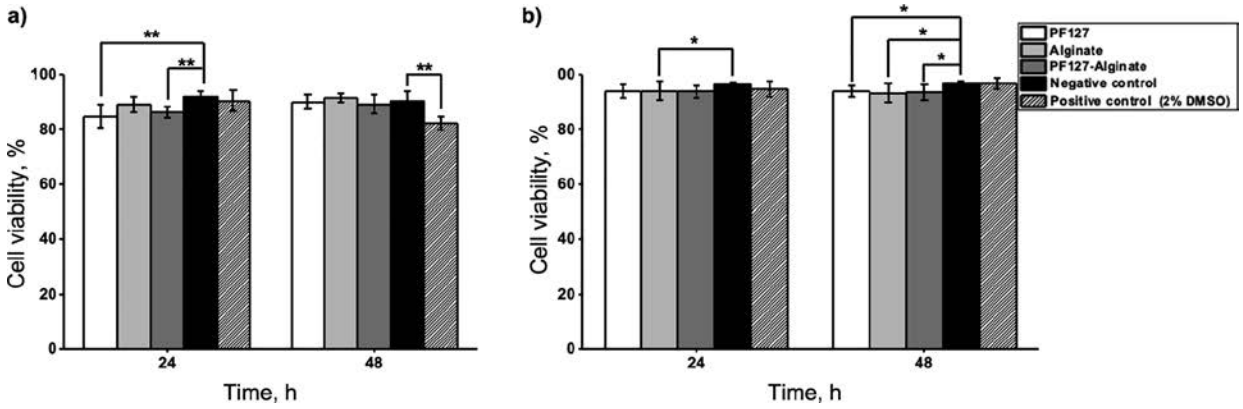

Figure 6. *In vitro* cytocompatibility of the PF127 20% w/v-alginate 1% w/v, PF127 20% w/v, and alginate 1% w/v hydrogels with (a) HeLa cells and (b) CRL-2616 cells. Data are presented as mean ± standard deviation ($n = 6$). $p < 0.05$ (*) and $p < 0.005$ (**).

other hand, Ca fluorescence X-rays (K_α 3.692 and K_β 4.013) were still detected in the hydrogels due to their residual presence as complexing factors in the alginate chains and in the SVF, in the form of $Ca(OH)_2$.

The AuNP release profile presented in Figure 5a is analyzed using the power-law model. Fitting the release curve to this model allowed the extraction of the n, k and r^2 parameters describing the release parameters for values up to 60% (Figure 5b).[41] The exponent n in this equation determines the underlying release mechanism: it is generally assumed that, if $n = 0.5$, then the release is controlled only by the diffusion of the encapsulated substance; if $n = 1$, then the release is controlled only by the degradation of the delivery matrix; if $0.5 < n < 1$, then the release is governed by both the diffusion of enclosed molecules and degradation of the matrix.[41] In the present study, an n value of 0.71 was found, with a squared correlation coefficient r^2 of 0.998. Therefore, it can be assumed that the release of AuNPs from the PF127-alginate hydrogel is controlled by both NP diffusion and material degradation mechanisms.

Swelling Ratio. Finally, the swelling ratio of the freeze-dried PF127-alginate hydrogel was evaluated in SVF at pH 4.5 (Figure 5c). The high initial slope of the swelling ratio curve indicates a high swelling rate. Swelling equilibrium was reached after 2 h of incubation, at about 4.6×. The mass swelling factor at equilibrium (MSF) of the PF127-alginate formulation was found to be 5.91 ± 0.23.

Hydrogel Biocompatibility and Bio-Functionality Tests: Cell Viability, Contact Assays, Mucin Adsorption, and Membrane Diffusion Tests. *Direct Cell Contact Assays.* According to the ISO 10993-5 guidelines, cytotoxicity tests can be of three (3) types: direct contact, extract dilution, and indirect contact tests.[42,43] The direct contact method, in which cell viability is measured by submitting the cells to the tested formulation, is the most sensitive one.[43] In the present study, the PF127-alginate system was tested using the trypan blue dye exclusion method, with human cervical cancer (HeLa), human normal vaginal mucosa (CRL 2616), and human breast cancer (BT-474) cell lines. The BT-474 cell line was selected to broaden the application spectrum of the PF127-alginate formulation; in fact, early-stage breast cancer therapies could also benefit from the development of the localized hydrogel delivery systems.[44]

The cell viabilities of the HeLa and CRL-2616 cells are shown in Figure 6, whereas the results of the experiment with BT-474 cells (breast cancer) can be found in the Supporting Information, Section S6, Figure S6. After 2 days in direct contact with the tested hydrogels, HeLa and CRL-2616 cells were viable at 90 and 93%, respectively, thus confirming the absence of obvious cytotoxicity. Moreover, PF127 and PF127-alginate formulations did not affect the proliferation of the HeLa and CRL-2616 cells, whereas alginate alone had a significant impact on the CRL-2616 cell proliferation activity (Supporting Information, Section S6, Figure S7), thus indicating the necessity to keep molecular ratios of alginate low. We hypothesize that the enhanced presence of microchannels in hydrogels previously loaded with high fractions of PF127 has a positive impact on nutrient and oxygen transport to the cells. It also improves cell-to-cell interactions that are critical for their proliferation.[18] Alginate alone, once cross-linked with Ca^{2+}, forms a more rigid and dense environment and has a much slower degradation rate. This could hamper nutrient mass transport as well as the space for the cells to deposit the extracellular matrix.

Mucin Adsorption Tests by the Mucin Glycoprotein Assay (PAS Staining). Mucoadhesive force is an important physicochemical parameter in the design of hydrogels for vaginal applications. Strong mucoadhesion properties help prevent the rapid drainage of the therapeutic gel from the membrane, thus prolonging the residence time at the administration site. The PAS method used in this study was introduced by Mantle and Allen in 1978.[45] The recent literature on PAS staining has mainly focused on the evaluation of mucoadhesive properties of nano/microparticles dispersed in aqueous solutions.[46,47] In the present study, a modified PAS staining protocol was applied to the semi-solid hydrogel system. To evaluate the percentage of mucins adsorbed on the gel surface, the concentration of free mucins in the solution after the incubation with the gel was quantified using a standard calibration curve (see Figure 2c). The gels were incubated with an aqueous mucin solution with a concentration of 100 μg/mL (gray triangle). The standard mucin samples with this concentration led to an absorbance level of 0.18 ± 0.02 a.u. at 575 nm. After performing PAS staining, an absorbance of 0.14 ± 0.02 a.u. was observed (blue circle), which corresponds to a concentration of 81.4 ± 13.2 μg/mL of free mucins. This value means that approximately 19% (about

https://doi.org/10.1021/acsbiomaterials.1c01399
ACS Biomater. Sci. Eng. 2022, 8, 1200−1214

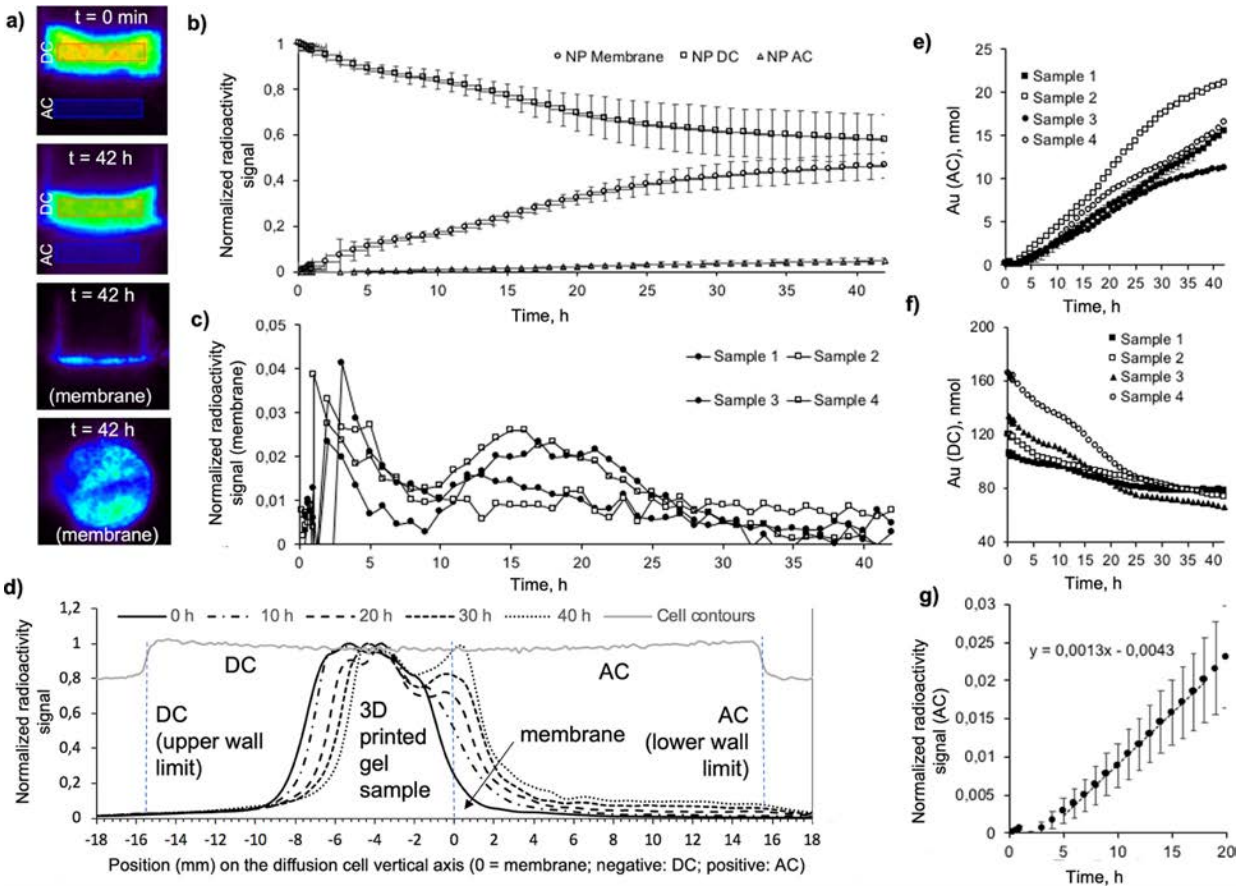

Figure 7. Permeation process across porcine vaginal membranes as visualized with PET imaging. (a) Sagittal PET images of the diffusion cell at t = 0 and 42 h, showing the accumulation of activity in the AC. Both ROIs corresponding to the area measured in the DC and to the AC are represented as rectangles. Sagittal and coronal PET images corresponding to the washed membranes at the end of the experiment, with both AC and DC compartments emptied, are also presented. (b) Radioactivity signal in the DC and in the AC and accumulating in the membrane over time normalized to the radioactivity signal in the DC at the beginning of the experiment. (c) Rate of AuNP accumulation in the membrane (radioactivity signal normalized to the intensity in the DC at the beginning of the experiment; four samples measured). (d) Radioactivity signal (normalized to the intensity in the DC at the beginning of the experiment) across the vertical axis of the diffusion cell. (e, f) Individual permeation profiles in the DC and in the AC (four samples measured) presented as the total amount of permeated Au (in nmol of Au per compartment). (g) The fit of the linear portion of the AC permeation profile reveals the lag time to permeation of the AuNPs across the vaginal membranes (average of four samples).

93 out of 500 μg) of the mucins in the solution were adsorbed on the gel surface, which demonstrates a strong mucoadhesive potential, suitable for intravaginal applications. For good mucoadhesive materials (*e.g.*, chitosan), adsorption rates of 23−28% are usually reported.[48]

Membrane Diffusion and Accumulation Tests by PET Imaging. A diffusion cell operated in a PET system was used to demonstrate the potential of the hydrogel to deliver NPs to the vaginal membrane and across. The permeation process was visualized by PET imaging, which provides real-time, high-sensitivity measurements of permeation processes across biological and synthetic membranes.[31,49] PET allowed to track the diffusion, permeation, and accumulation of Au NPs radiolabeled with zirconium-89 (^{89}Zr), in the vaginal mucous membrane. ^{89}Zr, with its physical half-life of $t_{1/2}$ = 78.41 h, is optimal to monitor systemic biodistribution of long-circulating drugs, NPs, and antibodies.[50−53]

The permeation process was recorded by PET for a period of 42 h, a duration that matches the time window of radiosensitization and photothermal therapy treatments that are being developed for cervical cancer.[39] Figure 7a displays cross sections of the diffusion cell compartments at the beginning (t = 0) and at the end of a 42 h permeation process. Radioactivity, serving in this case as a measure of AuNPs, progressively builds up in the AC while in parallel significantly decreases in the DC. The vaginal membrane itself demonstrated a very strong accumulation of AuNPs (Figure 7a, t = 42 h, membrane). Therefore, PET has the potential to become a key tool for monitoring the homogeneity of therapeutic NP accumulation in the vaginal wall during the application of an oncological treatment.

The normalized radioactivity signal in the DC is plotted in Figure 7b as a function of time. The profiles clearly show a strong release of AuNPs in the first 25 h followed by a decrease in the release rate. The amount of AuNPs permeated through the membrane in the AC in 42 h did not account for more than 5% of the total AuNPs initially present in the DC; in fact, a

https://doi.org/10.1021/acsbiomaterials.1c01399
ACS Biomater. Sci. Eng. 2022, 8, 1200−1214

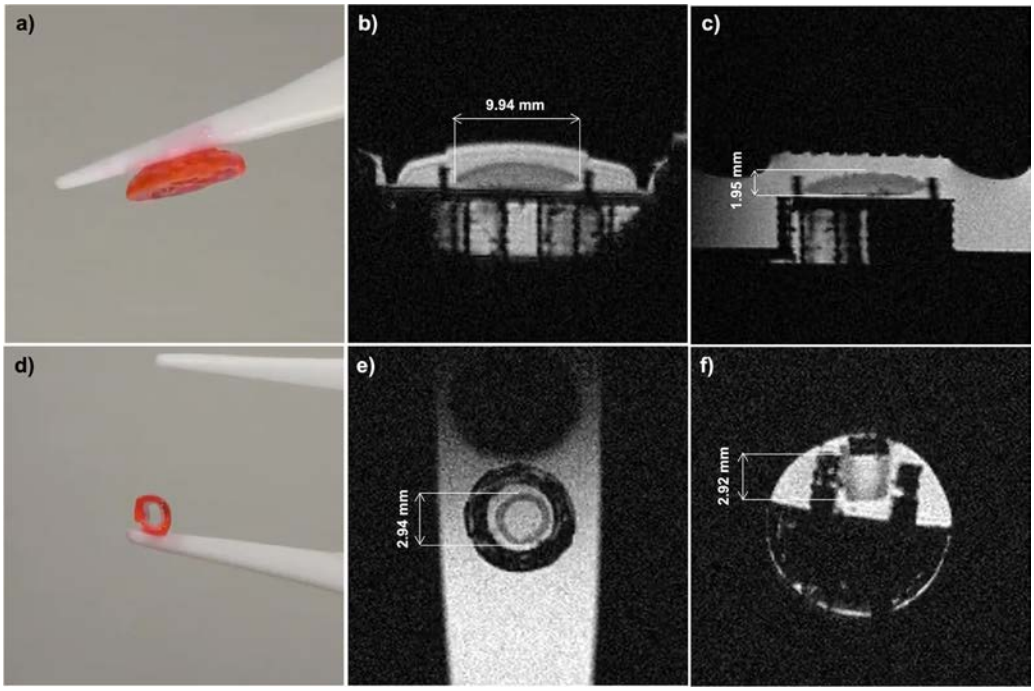

Figure 8. Photographs and MRI scans of the fabricated lens-shaped and hollow tube-shaped structures. (a, d) Photographs of the gel scaffolds after cross-linking; (b) axial view of the lens-shaped gel; (c) sagittal view of the lens-shaped gel; (e) coronal view of the hollow tube-shaped gel; (f) axial view of the hollow tube-shaped gel. All the images were obtained using a T1-weighted 2D spin echo sequence.

very strong accumulation was found in the membrane (averages of 38.3 and 46.7% at 25 and 42 h, respectively).

The rate of accumulation in the membrane is represented in Figure 7c. For each sample, a drastic increase is observed in the first few hours followed by a rapid drop; then, a resurgence of AuNP accumulation in the membrane is observed between t = 10 and 25 h. For each one of the hydrogel samples, the data from continuous PET acquisition allowed to extract a signal profile across the full vertical height of the diffusion cell (Figure 7d; sample 3 is shown). These profiles indicate the contraction of the hydrogel cylinder toward the membrane, following the depletion of the Pluronic content; this loss of the polymer (Pluronic dissolved and migrated into the AC) resulted in a contraction of the gel as revealed by a shift of the profile toward the right portion of the graph (Figure 7d). Also worth noticing is the steady increase in intensity at the membrane (position = 0 mm) from t = 0 up to 40 h.

The individual diffusion profiles acquired in the DC and in the AC (Figure 7e,f), each containing slightly different starting concentrations of Au, display similar behavior. A gradual increase in the Au concentration in the AC is the sign of AuNPs crossing the membrane (Figure 7e). In the DC (Figure 7f), an initial (0−5 h) strong decrease in the Au concentration could be probably attributed to the more rapid escape of AuNPs located close to the surface of the hydrogel in contact with the membrane. Then, the depletion of AuNPs in the vicinity of the membrane slows down this process, and a plateau is observed (5−10 h), which could correspond to the initiation of the Pluronic degradation process that progressively liberates AuNPs from the hydrogel scaffold (as shown in Figure 5a). The third step, occurring between t = 10 and 25 h (Figure 7f), is an acceleration of the AuNP release process, which corresponds to the strong release of Pluronic as measured in the same time period by physicochemical analysis (Figure 2b). Finally, after 25 h, the decrease in the Au concentration considerably slows down, and this indicates that the remaining fraction of AuNPs is either more "attached" to the alginate matrix or simply that this release process takes place in the full volume (thus slower). A lag time to the permeation across the membrane of 3.3 ± 1.5 h was found by fitting the linear portion of the AC permeation profile (Figure 7g). Based on a measured thickness of the vaginal membrane of 2.0 ± 0.5 mm, a diffusion coefficient (D_M) of 2.02 × 10^{-3} cm^2/h was calculated. Finally, the total concentration of AuNPs in the AC was 16.1 ± 3.5 nmol (after 42 h), and the total accumulation of AuNPs in the membrane was 34.6 ± 4.1 nmol or 11.0 ± 1.3 $nmol/cm^2$.

Printability Assessment of AuNP-Containing Hydrogels and Visualization with MRI. The printability of the hydrogel ink depends on the different properties such as its viscosity, surface tension, the mechanism of cross-linking, and the parameters of the 3D printing process (*e.g.*, applied pressure).[54] On the other hand, printing resolution is highly dependent on the inner diameter of the nozzle. The parameters of the 3D printing process were optimized for the PF127-alginate hydrogel scaffolds of two different shapes (Figure 8). A lens-shaped scaffold with a diameter of 10 mm represents a structure with simple geometry and can be used as a patch covering an affected area of the cervix, whereas a smaller hollow tube-shaped structure with an inner diameter of 3 mm was developed for eventual small animal studies. After immersion in $CaCl_2$ solution, the gel constructs retained their shapes and could be easily manipulated.

The accuracy of the printing process and reproducibility of the gel geometry were evaluated by MRI. By comparison with X-ray computed tomography (CT), which is an imaging

https://doi.org/10.1021/acsbiomaterials.1c01399
ACS Biomater. Sci. Eng. 2022, 8, 1200−1214

technique that does not delineate very well the contours of soft materials, MRI is based on the detection of ^{1}H protons, including from water. Therefore, it is a very convenient technique to evaluate the contours of hydrogels. The dimensions of the lens-shaped scaffolds were 9.94 ± 0.05 mm in diameter and 1.95 ± 0.02 mm in height. An average percent deviation was calculated as deviation from theoretical values (10 mm in diameter and 2 mm in height) and was found to be 0.5 and 0.75% for diameter and height, respectively. Thus, the gels demonstrated minimal deviation from the design (<1%), for both outer diameter and height.

For the smaller hollow tube-shaped gels, the diameter was found to be 2.94 ± 0.07 mm, and the height was equal to 2.92 ± 0.0 mm. Average percent deviations from theoretical values (3 mm in diameter and 3 mm in height) were calculated to be 2.4 and 2.1% for diameter and height, respectively.

The developed imaging methodology will be translated to *in vivo* studies in the mouse model to precisely track the process of hydrogel implant degradation *in vivo* after its administration.

DISCUSSION

Photothermal and brachytherapy applications are being developed for the treatment of cervical cancer that often require the topical administration of therapeutic nanoparticles.[55−57] In the PTT method, the absorption of light in the visible and near-infrared region by AuNPs leads to local heat generation, which induces damage to cancer cells.[58] In radiotherapy, AuNPs could be used as additives to enhance the effects of radiation on cancer tissues.[57,59,60] Moreover, in combination with chemotherapeutics (*e.g.*, doxorubicin), they represent an improved approach for cancer chemoradiotherapy.[12]

Hydrogel systems releasing NPs onto the vaginal mucosa for a certain period and according to patients' needs could enhance the efficacy of AuNPs used in these treatments. Preforming certain types of gels with a 3D printing approach could be advantageous for adjusting the shape of the topical delivery system to the anatomy of the patient and the specifics of the pathology. In the present study, a hydrogel formulation composed of Pluronic F127 and alginate with optimal 3D printing properties was developed, optimized, and evaluated for its degradation and AuNP-releasing properties in the context of cervical cancer.

We found that the degradation of the Pluronic F127-alginate-AuNP gel was governed mainly by the rapid dissolution of the PF127 component out of the polymer network.[35] In this work, the established mechanism of the PF127-alginate degradation demonstrates that the ionic cross-linking of alginate by Ca^{2+} ions provides higher stability to this component in the degradation experiment, whereas the physical cross-linking of PF127 by weak hydrophobic interactions results in quick disintegration of the polymer chains. Moreover, we found that the PF127-alginate gels were completely disintegrated on the sixth day of the degradation experiment, thus, from a clinical perspective, suggesting that no removal step would be necessary.

Ideally, AuNPs delivered on the cervical cancer site should be released not too quickly yet within a few days to avoid unnecessarily extended hospitalization of the patients. This study demonstrated that ∼80% of encapsulated AuNPs was released after 2 days of incubation. In PF127 formulations, the release of encapsulated drugs is usually controlled by hydrogel degradation.[37] Once exposed to the release medium, PF127 gels dissolve very fast, leading to a dissolution-controlled burst release of enclosed therapeutics. Adding alginate to the system provides structural stability while delaying degradation. In the case of the PF127-alginate blend, both hydrogel dissolution and nanoparticle diffusion are the main release factors. The higher swelling index of the PF127-alginate formulation than PF127 alone also leads to increased diffusional path length for AuNPs.[61]

Adhesion of the hydrogel to the mucosal wall is essential to prolong its residence time in the vagina; thus, mucoadhesive properties must be carefully measured. In the present study, the swelling potential of the polymers was reported to play a crucial role in their bioadhesive behavior. In general, mucoadhesion increases to a certain extent along with the degree of hydration.[62] However, excessive swelling results in an abrupt drop of hydrogel adhesiveness. Usually, a moderate swelling behavior reduces gel detachment from the mucus, thus prolonging adhesion duration.[63] In this study, the MSF of the PF127-alginate gel was found to be 5.91 ± 0.23. This value favorably compares with the MSFs reported in the literature for polyacrylic acids (Carbopol 974P NF and Noveon AA-1; ∼5.5−6.5). Those are well known for their high mucoadhesive potential and, therefore, widely used in the pharmaceutical industry for vaginal applications.[63]

The mucoadhesive potential of the PF127-alginate hydrogel was evaluated by PAS staining, which revealed that 19% of mucins are adsorbed on the gel's surface after 1 h. As a comparison, a previous study showed that about 23−28% of mucins were adsorbed on chitosan microspheres prepared by glutaraldehyde cross-linking, which are known for their high mucoadhesive potential.[48] Therefore, through its two main components, the PF127-alginate gel demonstrated relatively strong mucoadhesive properties, suitable for intravaginal applications. The carboxylic acid moieties present in the alginate molecules interact with mucins by hydrogen bonding.[20] Alginate mucoadhesion also depends on the molecular weight of the polymer. In general, it has been shown that the bioadhesive strength of a polymer increases with molecular weights above 100,000 g/mol.[64] In this study, we used alginate with an M_w of 120,000−190,000 g/mol. Smaller molecules are often associated with more rigid and, thus, poorly adhesive interactions upon contact with the mucosal membrane. Pluronic F127 being a non-ionic neutral polymer is considered less adhesive than anionic alginate.[65] However, Pluronic features hydrophilic oxide groups in poly(ethylene oxide) blocks, which can interact with oligosaccharide chains of the mucins via hydrogen bonding.[66] It is worth noting that the gel formulation used in this work can interact with mucins via non-specific hydrogen bonding and hydrophobic interactions only that are much weaker than covalent bonding.[67] Should this prove necessary in the future for *in vivo* studies and in the perspective of translational clinical applications, the mucoadhesive properties of the Pluronic-alginate formulation could be further enhanced by addition of polymers facilitating covalent bonding with mucin glycoproteins. Disulfide bonds could prove useful as well as polymers that can provide more sites for non-specific hydrogen bonding (polyethylene oxide and polycarbophil).[62,67]

The diffusion cell experiments performed with the porcine vaginal mucosa membrane using PET imaging revealed the kinetics of AuNP release from the hydrogel, their accumulation in the membrane, and permeation across it and into the AC. PET is ∼1000 times more sensitive than spectroscopic

https://doi.org/10.1021/acsbiomaterials.1c01399
ACS Biomater. Sci. Eng. 2022, 8, 1200−1214

analytical techniques usually employed for diffusion cell measurements, and it allows a continuous acquisition of a signal for a period of several days.[31,49] Overall, the diffusion cell results demonstrated that a very large fraction (47%) of AuNPs accumulated in the membrane after 42 h. This is a very significant result since potential toxicity of AuNPs to the uterus and other healthy tissues should be considered at all steps in the development of future cervical cancer therapies.[55−57] The gradual liberation of AuNPs from the hydrogel, coupled to their very strong retention at the membrane site, is in agreement with the requirements of AuNP administration locally prior to photothermal and radiosensitization procedures.

Finally, the hydrogel system can be easily 3D printed in different forms. Not only this behavior eliminates several forming limitations of the existing thermosensitive in situ forming gel formulations, but it can also provide a significant step toward personalized medicine. Only a few examples have been reported until now of 3D printed vaginal rings made of polymers.[68,69] To our knowledge, the present study provides the first example of a 3D printing technology applied to the fabrication of a nanoparticle-eluting hydrogel delivery system for the treatment of cervical cancer. The very high geometrical compliance of the 3D printed objects as shown by MRI provides a strong proof of concept for the design of pre-clinical *in vivo* experiments.

CONCLUSIONS

This study aimed at developing a hydrogel formulation optimized for the delivery of nanoparticles at the vaginal mucosal wall, which could also express good properties in 3D printing. A Pluronic F127-alginate hydrogel formulation was developed, revealing a high adsorption of mucins and allowing the release of ultrasmall AuNPs over a period of several hours, thus matching the requirements for radiosensitizing agents in cervical cancer brachytherapy. The hydrogel formulation was tested for cytocompatibility in three cell lines, and the release of AuNPs from the hydrogel and their accumulation in vaginal membranes were quantitatively measured *in vitro*/*ex vivo* with a highly sensitive imaging modality, allowing real-time imaging (PET). Finally, the 3D printing properties of the AuNP-containing Pluronic F127-alginate hydrogel were demonstrated, and the geometrical precision of 3D printed objects prepared for translational applications was measured by MRI. This study demonstrates the high potential of Pluronic F127-alginate formulations for topical applications of 3D printed NP-releasing systems for vaginal membrane treatments, particularly, for photothermal and radiosensitizing applications involving AuNPs.

Nanoparticle-eluting hydrogel systems adapted to the specific anatomy of a patient could be developed for application at the cervix area affected by the malignancy or the tumor cavity after the resection. The design of these objects would be facilitated by MRI scans from the patients, which could form the basis of the computer aided designs necessary for the 3D printing software used to create anatomically relevant hydrogel delivery systems.

ASSOCIATED CONTENT

Supporting Information

The Supporting Information is available free of charge at https://pubs.acs.org/doi/10.1021/acsbiomaterials.1c01399.

Section S1: AuNP synthesis, characterization, and radiolabeling; Section S2: the gelation time test of the Pluronic F127 polymer solutions; Section S3: hydrogel degradation study with SEM; Section S4: micro-X-ray fluorescence imaging of AuNP-containing hydrogels; Section S5: *in vitro* release of AuNPs; Section S6: cell viability tests; Section S7: mucin adsorption tests; and Section S8: membrane diffusion and accumulation tests by PET imaging (PDF)

AUTHOR INFORMATION

Corresponding Author

Marc-André Fortin − *Département de Génie des Mines, de la Métallurgie et des Matériaux, Centre de Recherche sur les Matériaux Avancés (CERMA), Université Laval, Québec G1V 0A6, Canada; Axe Médecine Régénératrice, Centre de Recherche du CHU de Québec − Université Laval, Québec G1V 4G2, Canada;* orcid.org/0000-0002-8601-466X; Email: marc-andre.fortin@gmn.ulaval.ca

Authors

Mariia Kiseleva − *Département de Génie des Mines, de la Métallurgie et des Matériaux, Centre de Recherche sur les Matériaux Avancés (CERMA), Université Laval, Québec G1V 0A6, Canada; Axe Médecine Régénératrice, Centre de Recherche du CHU de Québec − Université Laval, Québec G1V 4G2, Canada*

Mahmoud M. Omar − *Département de Génie des Mines, de la Métallurgie et des Matériaux, Centre de Recherche sur les Matériaux Avancés (CERMA), Université Laval, Québec G1V 0A6, Canada; Axe Médecine Régénératrice, Centre de Recherche du CHU de Québec − Université Laval, Québec G1V 4G2, Canada*

Élodie Boisselier − *Axe Médecine Régénératrice, Centre de Recherche du CHU de Québec − Université Laval, Québec G1V 4G2, Canada; Département d'Ophtalmologie, Faculté de Médecine, Centre de Recherche sur les 1022 Matériaux Avancés (CERMA) and CUO-Recherche, Université Laval, Québec G3K 1A3, Canada*

Svetlana V. Selivanova − *Faculty of Pharmacy, Université Laval, Québec G1V 0A6, Canada; Axe Oncologie, Centre de Recherche du CHU de Québec − Université Laval, Québec G1R 3S3, Canada*

Complete contact information is available at: https://pubs.acs.org/10.1021/acsbiomaterials.1c01399

Author Contributions

The manuscript was written through the contributions of the primary and corresponding authors. All authors have approved the final version of the manuscript.

Funding

This study was partially financed by the NSERC-Discovery program (M.-A.F. - RGPIN-2017-06173). M.K. received a fellowship from the NSERC-CREATE POND program (973111).

Notes

The authors declare no competing financial interest.

ACKNOWLEDGMENTS

The authors are grateful to the following researchers at CHU de Québec - Université Laval Research Center: Dr. Sébastien Fortin and Dr. René C. Gaudreault (Axe Oncologie) for

providing HeLa cells used in the cell viability experiments. Mrs. Vicky Dodier (Département de Génie des Mines, de la Métallurgie et des Matériaux, Université Laval) is acknowledged for her contribution to MP-AES analysis. PET studies were performed at the Small Animal Imaging platform (CHU de Québec - Université Laval Research Center).

■ ABBREVIATIONS

AC, acceptor compartment; AuNPs, gold nanoparticles; DC, donor compartment; DFO, deferoxamine; DLS, dynamic light scattering; DMEM, Dulbecco's modified Eagle's medium; DMSO, dimethyl sulfoxide; EDTA, ethylenediaminetetraacetic acid; FOV, field of view; FTIR, Fourier-transform infrared spectroscopy; HEPES, (4-(2-hydroxyethyl)-1-piperazineethanesulfonic acid); LCGT, low critical gelation temperature; micro-XRF, X-ray fluorescence; MP-AES, microwave plasma atomic emission spectrometry; MRI, magnetic resonance imaging; MSF, mass swelling factor at equilibrium; PAS, periodic acid/Schiff reagent; PBS, phosphate buffered saline; PEG, polyethylene glycol; PET, positron emission tomography; PTT, photothermal therapy; ROI, regions of interest; RPMI, Roswell Park Memorial Institute medium; SEM, scanning electron microscopy; SVF, simulated vaginal fluid; TEM, transmission electron microscopy; TLC, thin-layer chromatography; UCGT, upper critical gelation temperatures; UV−vis, ultraviolet−visible spectroscopy

■ REFERENCES

(1) Ordikhani, F.; Erdem Arslan, M.; Marcelo, R.; Sahin, I.; Grigsby, P.; Schwarz, J. K.; Azab, A. K. Drug Delivery Approaches for the Treatment of Cervical Cancer. *Pharmaceutics* **2016**, *8*, 23.
(2) Xu, S.; Du, X.; Feng, G.; Zhang, Y.; Li, J.; Lin, B.; Yang, L.; Fu, S.; Wu, J. Efficient inhibition of cervical cancer by dual drugs loaded in biodegradable thermosensitive hydrogel composites. *Oncotarget* **2018**, *9*, 282−292.
(3) Gupta, S.; Gupta, M. K. Possible role of nanocarriers in drug delivery against cervical cancer. *Nano Rev. Exp.* **2017**, *8*, 1335567.
(4) Wang, X.; Wang, J.; Wu, W.; Li, H. Vaginal delivery of carboplatin-loaded thermosensitive hydrogel to prevent local cervical cancer recurrence in mice. *Drug Delivery* **2016**, *23*, 3544−3551.
(5) Hodge, L. S.; Downs, L. S., Jr.; Chura, J. C.; Thomas, S. G.; Callery, P. S.; Soisson, A. P.; Kramer, P.; Wolfe, S. S.; Tracy, T. S. Localized delivery of chemotherapy to the cervix for radiosensitization. *Gynecol. Oncol.* **2012**, *127*, 121−125.
(6) Naumann, R. W.; Leath, C. A., III Advances in immunotherapy for cervical cancer. *Curr. Opin. Oncol.* **2020**, *32*, 481−487.
(7) Liu, Y.; Yang, F.; Feng, L.; Yang, L.; Chen, L.; Wei, G.; Lu, W. In vivo retention of poloxamer-based in situ hydrogels for vaginal application in mouse and rat models. *Acta Pharm. Sin. B* **2017**, *7*, 502−509.
(8) Bilensoy, E.; Çırpanlı, Y.; Şen, M.; Doğan, A. L.; Çalış, S. Thermosensitive mucoadhesive gel formulation loaded with 5-Fu: cyclodextrin complex for HPV-induced cervical cancer. *J. Inclusion Phenom. Macrocyclic Chem.* **2007**, *57*, 363−370.
(9) Collaud, S.; Peng, Q.; Gurny, R.; Lange, N. Thermosetting gel for the delivery of 5-aminolevulinic acid esters to the cervix. *J. Pharm. Sci.* **2008**, *97*, 2680−2690.
(10) Dumortier, G.; Grossiord, J. L.; Agnely, F.; Chaumeil, J. C. A review of poloxamer 407 pharmaceutical and pharmacological characteristics. *Pharm. Res.* **2006**, *23*, 2709−2728.
(11) Garg, S. T. K. R.; Vermani, K.; Garg, A.; Kaul, C. L.; Zaneveld, L. J. D. Compendium of Pharmaceutical Excipients for Vaginal Formulations. *Pharm. Technol.* **2001**, *25*, 14−24.
(12) Li, T.; Zhang, M.; Wang, J.; Wang, T.; Yao, Y.; Zhang, X.; Zhang, C.; Zhang, N. Thermosensitive Hydrogel Co-loaded with Gold Nanoparticles and Doxorubicin for Effective Chemoradiotherapy. *AAPS J.* **2016**, *18*, 146−155.
(13) Kempe, S.; Mäder, K. In situ forming implants - an attractive formulation principle for parenteral depot formulations. *J. Controlled Release* **2012**, *161*, 668−679.
(14) Tao, J.; Zhang, J.; Hu, Y.; Yang, Y.; Gou, Z.; Du, T.; Mao, J.; Gou, M. A conformal hydrogel nanocomposite for local delivery of paclitaxel. *J. Biomater. Sci., Polym. Ed.* **2017**, *28*, 107−118.
(15) Cho, H.; Jammalamadaka, U.; Tappa, K. Nanogels for Pharmaceutical and Biomedical Applications and Their Fabrication Using 3D Printing Technologies. *Materials* **2018**, *11*, 302.
(16) Jamróz, W.; Szafraniec, J.; Kurek, M.; Jachowicz, R. 3D Printing in Pharmaceutical and Medical Applications - Recent Achievements and Challenges. *Pharm. Res.* **2018**, *35*, 1.
(17) Pitto-Barry, A.; Barry, N. P. E. Pluronic® block-copolymers in medicine: from chemical and biological versatility to rationalisation and clinical advances. *Polym. Chem.* **2014**, *5*, 3291−3297.
(18) Armstrong, J. P. K.; Burke, M.; Carter, B. M.; Davis, S. A.; Perriman, A. W. 3D Bioprinting Using a Templated Porous Bioink. *Adv. Healthcare Mater.* **2016**, *5*, 1724−1730.
(19) Liu, Q.; Li, Q.; Xu, S.; Zheng, Q.; Cao, X. Preparation and Properties of 3D Printed Alginate(−)Chitosan Polyion Complex Hydrogels for Tissue Engineering. *Polymers (Basel)* **2018**, *10*, 664.
(20) Anil, A.; Sudheer, P. Mucoadhesive polymers: A review. *J. Pharm. Res.* **2018**, *17*, 47−55.
(21) Laprise-Pelletier, M.; Simão, T.; Fortin, M. A. Gold Nanoparticles in Radiotherapy and Recent Progress in Nanobrachytherapy. *Adv. Healthcare Mater.* **2018**, *7*, 1701460.
(22) Singh, P.; Pandit, S.; Mokkapati, V. R. S. S.; Garg, A.; Ravikumar, V.; Mijakovic, I. Gold Nanoparticles in Diagnostics and Therapeutics for Human Cancer. *Int. J. Mol. Sci.* **2018**, *19*, 1979.
(23) Zhang, C.; Yan, L.; Gu, Z.; Zhao, Y. Strategies based on metal-based nanoparticles for hypoxic-tumor radiotherapy. *Chem. Sci.* **2019**, *10*, 6932−6943.
(24) Dickerson, E. B.; Dreaden, E. C.; Huang, X.; El-Sayed, I. H.; Chu, H.; Pushpanketh, S.; McDonald, J. F.; El-Sayed, M. A. Gold nanorod assisted near-infrared plasmonic photothermal therapy (PPTT) of squamous cell carcinoma in mice. *Cancer Lett.* **2008**, *269*, 57−66.
(25) Soliman, G. M.; Fetih, G.; Abbas, A. M. Thermosensitive bioadhesive gels for the vaginal delivery of sildenafil citrate: in vitro characterization and clinical evaluation in women using clomiphene citrate for induction of ovulation. *Drug Dev. Ind. Pharm.* **2017**, *43*, 399−408.
(26) Schmolka, I. R. Block polymer non-ionic surfactants in textiles. *J. Am. Oil Chem. Soc.* **1982**, *59*, 322−327.
(27) Liu, Y.; Zhu, Y. Y.; Wei, G.; Lu, W. Y. Effect of carrageenan on poloxamer-based in situ gel for vaginal use: Improved in vitro and in vivo sustained-release properties. *Eur. J. Pharm. Sci.* **2009**, *37*, 306−312.
(28) Ma, H.; He, C.; Cheng, Y.; Yang, Z.; Zang, J.; Liu, J.; Chen, X. Localized Co-delivery of Doxorubicin, Cisplatin, and Methotrexate by Thermosensitive Hydrogels for Enhanced Osteosarcoma Treatment. *ACS Appl. Mater. Interfaces* **2015**, *7*, 27040−27048.
(29) Suntornnond, R.; Tan, E. Y. S.; An, J.; Chua, C. K. A highly printable and biocompatible hydrogel composite for direct printing of soft and perfusable vasculature-like structures. *Sci. Rep.* **2017**, *7*, 16902.
(30) Schneider, T.; Westermann, M.; Glei, M. In vitro uptake and toxicity studies of metal nanoparticles and metal oxide nanoparticles in human HT29 cells. *Arch. Toxicol.* **2017**, *91*, 3517−3527.
(31) Omar, M. M.; Laprise-Pelletier, M.; Chevallier, P.; Tuduri, L.; Fortin, M.-A. High-Sensitivity Permeation Analysis of Ultrasmall Nanoparticles Across the Skin by Positron Emission Tomography. *Bioconjugate Chem.* **2021**, *32*, 729−745.
(32) George, E.; Liacouras, P.; Rybicki, F. J.; Mitsouras, D. Measuring and Establishing the Accuracy and Reproducibility of 3D Printed Medical Models. *Radiographics* **2017**, *37*, 1424−1450.

(33) Müller, M.; Becher, J.; Schnabelrauch, M.; Zenobi-Wong, M. Nanostructured Pluronic hydrogels as bioinks for 3D bioprinting. *Biofabrication* **2015**, *7*, No. 035006.
(34) Chung, Y. M.; Simmons, K. L.; Gutowska, A.; Jeong, B. Sol-gel transition temperature of PLGA-g-PEG aqueous solutions. *Biomacromolecules* **2002**, *3*, 511−516.
(35) Gioffredi, E.; Boffito, M.; Calzone, S.; Giannitelli, S. M.; Rainer, A.; Trombetta, M.; Mozetic, P.; Chiono, V. Pluronic F127 Hydrogel Characterization and Biofabrication in Cellularized Constructs for Tissue Engineering Applications. *Procedia CIRP* **2016**, *49*, 125−132.
(36) Rafael, D.; Andrade, F.; Martinez-Trucharte, F.; Basas, J.; Seras-Franzoso, J.; Palau, M.; Gomis, X.; Peréz-Burgos, M.; Blanco, A.; López-Fernández, A.; Vélez, R.; Abasolo, I.; Aguirre, M.; Gavaldà, J.; Schwartz, S., Jr. Sterilization Procedure for Temperature-Sensitive Hydrogels Loaded with Silver Nanoparticles for Clinical Applications. *Nanomaterials* **2019**, *9*, 380.
(37) Liu, Y.; Lu, W. L.; Wang, H. C.; Zhang, X.; Zhang, H.; Wang, X. Q.; Zhou, T. Y.; Zhang, Q. Controlled delivery of recombinant hirudin based on thermo-sensitive Pluronic (R) F127 hydrogel for subcutaneous administration: In vitro and in vivo characterization. *J. Controlled Release* **2007**, *117*, 387−395.
(38) Bodratti, A. M.; Alexandridis, P. Formulation of Poloxamers for Drug Delivery. *J Funct. Biomater.* **2018**, *9*, 11.
(39) Banerjee, R.; Kamrava, M. Brachytherapy in the treatment of cervical cancer: a review. *Int. J. Women's Health* **2014**, *6*, 555−564.
(40) Gaharwar, A. K.; Peppas, N. A.; Khademhosseini, A. Nanocomposite Hydrogels for Biomedical Applications. *Biotechnol. Bioeng.* **2014**, *111*, 441−453.
(41) Ci, T.; Chen, L.; Yu, L.; Ding, J. Tumor regression achieved by encapsulating a moderately soluble drug into a polymeric thermogel. *Sci. Rep.* **2015**, *4*, 1.
(42) Li, W.; Zhou, J.; Xu, Y. Study of the in vitro cytotoxicity testing of medical devices. *Biomed. Rep.* **2015**, *3*, 617−620.
(43) Srivastava, G. K.; Alonso-Alonso, M. L.; Fernandez-Bueno, I.; Garcia-Gutierrez, M. T.; Rull, F.; Medina, J.; Coco, R. M.; Pastor, J. C. Comparison between direct contact and extract exposure methods for PFO cytotoxicity evaluation. *Sci. Rep.* **2018**, *8*, 1425.
(44) Singh, S. K.; Singh, S.; Lillard, J. W., Jr.; Singh, R. Drug delivery approaches for breast cancer. *Int. J. Nanomed.* **2017**, *Volume 12*, 6205−6218.
(45) Mantle, M.; Allen, A. A colorimetric assay for glycoproteins based on the periodic acid/Schiff stain. *Biochem. Soc. Trans.* **1978**, *6*, 607−609.
(46) Lian, H.; Zhang, T.; Sun, J.; Liu, X.; Ren, G.; Kou, L.; Zhang, Y.; Han, X.; Ding, W.; Ai, X.; Wu, C.; Li, L.; Wang, Y.; Sun, Y.; Wang, S.; He, Z. Enhanced Oral Delivery of Paclitaxel Using Acetylcysteine Functionalized Chitosan-Vitamin E Succinate Nanomicelles Based on a Mucus Bioadhesion and Penetration Mechanism. *Mol. Pharmaceutics* **2013**, *10*, 3447−3458.
(47) Ouellette, M.; Masse, F.; Lefebvre-Demers, M.; Maestracci, Q.; Grenier, P.; Millar, R.; Bertrand, N.; Prieto, M.; Boisselier, É. Insights into gold nanoparticles as a mucoadhesive system. *Sci. Rep.* **2018**, *8*, 14357.
(48) Dhawan, S.; Singla, A. K.; Sinha, V. R. Evaluation of mucoadhesive properties of chitosan microspheres prepared by different methods. *AAPS PharmSciTech* **2004**, *5*, 112.
(49) Omar, M. M.; Laprise-Pelletier, M.; Lemay, S.; Lagueux, J.; Tuduri, L.; Fortin, M. A. A diffusion cell adapted to nuclear imaging instruments for the measurement of molecular release and pharmacokinetics across membranes. *J. Controlled Release* **2021**, *337*, 00356−00675.
(50) Carmon, K. S.; Azhdarinia, A. Application of Immuno-PET in Antibody-Drug Conjugate Development. *Mol. Imaging* **2018**, *17*, 1536012118801223.
(51) Deri, M. A.; Zeglis, B. M.; Francesconi, L. C.; Lewis, J. S. PET imaging with Zr-89: From radiochemistry to the clinic. *Nucl. Med. Biol.* **2013**, *40*, 3−14.
(52) Heskamp, S.; Raavé, R.; Boerman, O.; Rijpkema, M.; Goncalves, V.; Denat, F. Zr-89-Immuno-Positron Emission Tomography in Oncology: State-of the-Art Zr-89 Radiochemistry. *Bioconjugate Chem.* **2017**, *28*, 2211−2223.
(53) Jalilian, A. R.; Osso, J. A. Production, applications and status of zirconium-89 immunoPET agents. *J. Radioanal. Nucl. Chem.* **2017**, *314*, 7−21.
(54) Gopinathan, J.; Noh, I. Recent trends in bioinks for 3D printing. *Biomater. Res.* **2018**, *22*, 11.
(55) Amani, S.; Mehdizadeh, A.; Movahedi, M. M.; Keshavarz, M.; Koosha, F. Investigation of the Dose-Enhancement Effects of Spherical and Rod-Shaped Gold Nanoparticles on the HeLa Cell Line. *Galen Med. J.* **2020**, *9*, No. e1581.
(56) Liao, S.; Yue, W.; Cai, S.; Tang, Q.; Lu, W.; Huang, L.; Qi, T.; Liao, J. Improvement of Gold Nanorods in Photothermal Therapy: Recent Progress and Perspective. *Front. Pharmacol.* **2021**, *12*, 781.
(57) Yadav, P.; Bandyopadhyay, A.; Chakraborty, A.; Islam, S. M.; Sarkar, K. Enhancing the radiotherapeutic index of gamma radiation on cervical cancer cells by gold nanoparticles. *Gold Bull.* **2019**, *52*, 185−196.
(58) Rostami, A. S. A. Gold nanoparticles as cancer theranostic agents. *Nanomed. J.* **2019**, *6*, 147−160.
(59) Haume, K.; Rosa, S.; Grellet, S.; Śmiałek, M. A.; Butterworth, K. T.; Solov'yov, A. V.; Prise, K. M.; Golding, J.; Mason, N. J. Gold nanoparticles for cancer radiotherapy: a review. *Cancer Nanotechnol.* **2016**, *7*, 8.
(60) Song, K.; Xu, P.; Meng, Y.; Geng, F.; Li, J.; Li, Z.; Xing, J.; Chen, J.; Kong, B. Smart gold nanoparticles enhance killing effect on cancer cells. *Int. J. Oncol.* **2013**, *42*, 597−608.
(61) Hassan, A. S.; Soliman, G. M.; Ali, M. F.; El-Mahdy, M. M.; El-Gindy, G. E.-D. A. Mucoadhesive tablets for the vaginal delivery of progesterone: in vitro evaluation and pharmacokinetics/ pharmacodynamics in female rabbits. *Drug Dev. Ind. Pharm.* **2018**, *44*, 224−232.
(62) de Araujo Pereira, R. R.; Bruschi, M. L. Vaginal mucoadhesive drug delivery systems. *Drug Dev. Ind. Pharm.* **2012**, *38*, 643−652.
(63) Rojewska, M.; Olejniczak-Rabinek, M.; Bartkowiak, A.; Snela, A.; Prochaska, K.; Lulek, J. The wettability and swelling of selected mucoadhesive polymers in simulated saliva and vaginal fluids. *Colloid Surf., B* **2017**, *156*, 366−374.
(64) Salamat-Miller, N.; Chittchang, M. M.; Johnston, T. P. The use of mucoadhesive polymers in buccal drug delivery. *Adv. Drug Delivery Rev.* **2005**, *57*, 1666−1691.
(65) Partenhauser, A.; Bernkop-Schnürch, A. Mucoadhesive polymers in the treatment of dry X syndrome. *Drug Discovery Today* **2016**, *21*, 1051−1062.
(66) Ibrahim, E. A.; Ismail, S.; Fetih, G.; Shaaban, O.; Hassanein, K.; Abdellah, N. Development and characterization of thermosensitive pluronic-based metronidazole in situ gelling formulations for vaginal application. *Acta Pharm.* **2012**, *62*, 59−70.
(67) Xu, G.; Cheng, L.; Zhang, Q.; Sun, Y.; Chen, C.; Xu, H.; Chai, Y.; Lang, M. In situ thiolated alginate hydrogel: Instant formation and its application in hemostasis. *J. Biomater. Appl.* **2016**, *31*, 721−729.
(68) Fu, J.; Yu, X.; Jin, Y. 3D printing of vaginal rings with personalized shapes for controlled release of progesterone. *Int. J. Pharm.* **2018**, *539*, 75−82.
(69) Welsh, N. W. M.; Malcolm, K.; Devlin, B.; Boyd, P. 3D Printing of Microbicide Vaginal Rings: A Proof-of-Concept Study. *AIDS Research and human retroviruses* **2016**, *32*, 114.